UNIVERSIDADE DA BEIRA INTERIOR
Ciências Sociais e Humanas

The assessment of a world-ranked wheelchair sprinter aerodynamics analysis by computer fluid dynamics

Pedro Miguel Gomes Forte

Tese para obtenção do Grau de Doutor em
Ciências do Desporto
(3º ciclo de estudos)

Orientador: Prof. Doutor Daniel A. Marinho
Orientador: Prof. Doutor Tiago M. Barbosa

Covilhã, julho de 2018

“Pouco conhecimento faz com que as pessoas se sintam orgulhosas. Muito conhecimento, que se sintam humildes…”.

Leonardo Da Vinci

Academic thesis submitted with the purpose of obtaining a doctoral degree in Sport Sciences according to the provisions of Portuguese Decree-Law 107/2008 of 25 June.

Funding

This thesis was supported by National Funds through FCT - Portuguese Foundation for Science and Technology (UID/DTP/04045/2013) - and the European Fund for regional development (FEDER) allocated by European Union through the COMPETE 2020 Programme (POCI-01-0145-FEDER-006969).

Acknowledgments

First of all, I would like to thanks the Sports Department of the University of Beira Interior. Without all the members and this institution this work would not be the same.

Second, thanks to Professors Daniel Marinho and Tiago Barbosa for their supervision. Without them this work was not possible to be concluded. Thank you for your exceptional knowledge and patience.

To professors Pedro Morouço and Jorge Morais for their contribution to my academic formation, to provide me solutions and for their attention in these years. A special thanks also to professor Jorge Morais to follow my formation along the last five years.

To my girlfriend Lúcia Ribeiro, for her patience in this work development, to believe and encourage me. Thanks for your affection, you were always there. Even more, without you this work was not possible to be concluded.

To my family, specially parents and brother. To my parents for the values they had transmitted to me, my education and for the men they helped me to be. To my brother, for the example of perseverance. Thanks for teaching me that, when it depends of us, it will be become truth for sure. To my grandmother for all the worries with me. Finally, my aunt Maria José, you helped me a lot during my academic formation. Thanks to all.

To my friends and colleges, Eric, Marisa, Flávio and Ana. Thank you Pe. José Antonio, we do know how much you helped me, thanks for the conversations, the worries and the presence. To all that i did not refer but that encouraged me to proceed the studies, for asking and worry with me. Thank you.

List of Publications

This doctoral thesis is supported by the following publications:

Forte, Pedro; Marinho, Daniel A; Barbosa, Tiago M. (2015). Technologic Appliance and Performance Concerns in Wheelchair Racing – Helping Paralympic Athletes to Excel. *New Perspectives in Fluid Dynamics*, ed. Chaoqun Liu, 101 - 121. ISBN: 978-953-51-2228-9. Rijeka: InTech.

Forte, Pedro; Marinho, Daniel A; Morouço, Pedro; Barbosa, Tiago M. (2016). CFD analysis of head and helmet aerodynamic drag to wheelchair racing. *1st International Conference on Technology and Innovation in Sports, Health and Wellbeing (TISHW)*, 1-6.

Forte, Pedro; Marinho, Daniel A; Morais, Jorge E; Morais; Morouço, Pedro G; Barbosa, Tiago M. (2016). Comparison by computer fluid dynamics of the drag force acting upon two helmets for wheelchair racers. *AIP Conference Proceedings 1863(1): 520005 – 520008.*

Forte, Pedro; Marinho, Daniel A; Morais, Jorge E; Morouço, Pedro G; Barbosa, Tiago M. 2018. "The variations on the aerodynamics of a world-ranked wheelchair sprinter in the key-moments of the stroke cycle: A numerical simulation analysis", PLOS ONE 13, 2: e0193658 - e0193658.

Forte, Pedro; Marinho, Daniel A; Morais, Jorge E; Morais; Morouço, Pedro G; Barbosa, Tiago M. (2018). Estimation of mechanical power and energy cost in elite wheelchair racing by analytical procedures and numerical simulations. *Computer Methods in Biomechanics and Biomedical Engineering.*

Resumo

A analise da aerodinâmica desempenha um papel determinante nas provas de velocidade em cadeiras de rodas. Assim, o objetivo desta tese passou por analisar a aerodinâmica de um sujeito das provas de velocidade em cadeiras de rodas, com recurso à análise computacional de fluidos. Para tal, foram realizados quatro estudos, uma revisão de literatura e três estudos empíricos. Foram objetivos dos estudos: (i) rever a literatura quanto ao estudo da aerodinâmica das provas de velocidade em cadeiras de rodas; (ii) comparação de dois capacetes do tipo contrarrelógio e pista em duas posições (olhar em frente e olhar para baixo); (iii) comparação aerodinâmica entre as diferentes fases de um ciclo de puxada com recurso às simulações numéricas; (iv) estimativa da potência mecânica e custo energético num sprinter das provas de velocidade em cadeiras de rodas através de procedimentos analíticos e simulações numéricas. As principais conclusões obtidas foram que: (i) existe pouca literatura e conhecimento acerca das provas de velocidade em cadeiras de rodas, nomeadamente no estudo da aerodinâmica com recurso às simulações numéricas; (ii) os capacetes contrarrelógio são mais efetivos desde que o atleta mantenha o olhar em frente tanto quanto possível; (iii) a aerodinâmica de um atleta das provas de velocidade em cadeiras de rodas variou nas diferentes fases do ciclo de puxada; (iv) a potência mecânica e custo energético foram maiores na fase da pegada, seguida da largada e por fim a fase de recuperação. A principal conclusão desta tese é que torna-se possível melhorar a aerodinâmica de um sujeito das provas de velocidade em cadeiras de rodas através do correto uso do capacete ideal e mantendo tanto quanto possível o alinhamento e sincronização corporal durante as puxadas.

Palavras-chave

Paralimpico, forças resistivas, biomecânica, cinética, equipamentos, técnica.

Abstract

Aerodynamics can play an important role in the performance of a wheelchair spinter. The aim of this thesis was to analyse the aerodynamics of a wheelchair sprinter by computer fluid dynamics. This thesis comprises a series of four studies (a review of the literature and three empirical studies). The studies aimed to: (i) review the literature on aerodynamics in wheelchair racing; (ii) compare two different helmets (road vs time trial) at several speeds and head positions by CFD. (iii) assess the aerodynamics in different key-moments of the stroke cycle by CFD; (iv) compare the mechanical power and energy cost of transportation delivered by an elite wheelchair sprinter in key-moments of the stroke cycle. The main conclusions were: (i) there is a lack of research on wheelchair racing aerodynamic's assess by CFD; (ii) a time trial helmet imposed lower drag keeping a neck hyperextension; (iii) the aerodynamics of a wheelchair racing athlete varied over the different phases of the stroke cycle; (iv) the mechanical power and energy cost in elite wheelchair racing varied in different phases of the stroke cycle. The main conclusion of this thesis was that it is possible to enhance the aerodynamics of a wheelchair sprinter by selecting the best sport garement and equipment, as well as keeping a good body alignment in the key-phases of the stroke cycle.

Keywords

Paralympics, resistive forces, biomechanics, kinetics, equipment, technique.

Table of Contents

List of Figures

List of Tables

List of Abbreviations

ACd	Effective surface area
Ad	Surface area
C	Energy Cost
CCD	Coast-down distance
Cd	Drag coefficient
CFD	Computer fluid dynamics
CR	Rolling coefficient
FA	Applied force by the ground on the rear wheels
Fd	Drag force
FI	Inertial force
gr	Grams
k	Kinetic energy
Kg	Kilograms
m	Meters
N	Newtons
Pd	Power to overcome drag
Pext	External Mechanical Power
Ptot	Total Power
RANS	Reynolds-Averaged Navier-Stokes
S	Seconds
W	Watts

Chapter 1. General Introduction

1.1. Background

There is a concern about not to include people with disabilities in several areas of society (Duarte & Santos, 2003). Sports play an important role in including people with disabilities in the society (Paciorek, 2004; Winnick, 2004).

Wheelchair sports appeared after World War II. The first wheelchair games were organized in 1948. In 1952 were organized the first international wheelchair sporting competition for disable people (Cooper, 1990). Wheelchair racing was recognized as an Olympic sport in 1986. Paralympics are the major event for athletes with disabilities. Now, every race detail may help athletes to excel and define new strategies. The subject participations are in accordance to their category and injury type in spine C5-6, C7-8, T1-7e T8-S4 for the classes T51, T52, T53 and T54 respectively (IPC, 2007).

In wheelchair racing, the athlete had to push the handrim to generate motion (Cooper, 1990; Fuss, 2009; Forte, Marinho and Barbosa, 2015). It is possible to divid the stroke cycle in propulsion and and recovery. The propulsive moment is subdivided in: the catch phase (the hand contact moment on the handrim, usually near 12 and 14 o'clock); drive (is the moment that the hand wrist acceleration on the handrim); and release phase (the time period that the hand does not contact on the handrim) (Fuss, 2009). The recovery moment is the period of time between the release moment and a new catch moment. During the two moments is possible to observe three or four equilibrium horizontal forces. During the propulsion it is possible to observe the inertial force in negative direction in pair with drag and rolling friction force. The generated force by the ground on the rear wheel as a positive direction. In the recovery phase, the forces are the rolling resistance, aerodynamic drag and inertial (Petrushov, 1998; Fuss, 2009). Thus, to reach a higher acceleration, the inertial force and the ground force on the rear wheels must be maximized. The rolling friction and drag must be minimized to sooner reach and maintain the maximal speed. Then, it is possible to observe that drag plays an important role in athlete's performance.

1.2. Aerodynamics

In wheelchair racing, drag plays an important role in athlete's performance (LaMere & Labanowich, 1984; Candau et al., 1999; di Prampero, 1986; Martin et al., 2006; Millet and

Candau, 2002). At world record speed, drag force may account by 34.89% of the overall resistive forces (Barbosa et al., 2014). The aerodynamics of the wheelchair-athlete system, is mainly determined by the frontal area and the subject's posture. The drag area in racing wheelchairs ranges between 0.123 and 0.145 m^2 (Fuss, 2009).

The rolling friction and drag encompasses the resistive forces. The drag reduction will minimize the resistive forces. For that, during the race, some athlete's concerns are the head and body alignment (Barbosa et al., 2016). Equipment's such as helmets may help to reduce the aerodynamic drag. The ideal body position may also contribute about 10% for aerodynamic drag reduction (Harder et al. 2010). Reducing the drag, athlete's will need less effort to reach the maximal speed.

1.3. Drag Assessment by Computer Fluid Dynamics

It is possible to measure the aerodynamic drag by analytical procedures, experimental tests and numerical simulations by computer fluid dynamics (CFD) (Forte, Marinho and Barbosa, 2015). CFD is a biomechanics subarea that analyses the fluid flow behaviour around an object. This methodology consists in the discretization of Navier-Stokes equations by the finite volumes approach. These equations are underpinned by Newton's second law of fluid mechanics. It is assumed that the fluid stress is the sum of its viscosity diffusion resulted from the applied pressure term. The equations solution determines the fluid velocity in a given space and time moment. Then, CFD is based in one approximated finite volume. The space is subdivided in small particles intending to generate a mesh of greed. Then, an algorithm is applied to resolve the volume motion equations (Marinho, et al., 2012). CFD can be used to predict the fluid flow behaviour, the mass and hot transference, chemic reactions and other related issues. This analysis allows to answer different questions without resource to experimental tests. CFD can provide a bridge between theory and practice and could be used for aerodynamics studies (Lyttle & Keys, 2006).

In sports sciences, CFD has presented validity and accuracy in different fluids, bodies and tasks in sports. It has been validated and classified as feasible in hydro and aerodynamics testing (Liu, 2002). CFD has been presented as a valid and appropriated instrument assess aerodynamics and to simulate wind tunnel testing (Forte, Barbosa & Marinho, 2015; Dabnichki & Avital, 2006).

CFD is a reproducible methodology, in experimental tests the outputs may depend of several factors. This does not occur in numerical simulations where the output depends only from the input (Dabnichki & Avital, 2006).

1.4. Research Gap

The athlete's posture and equipment's use seem to influence drag. To better understand the equipment's and posture influence on drag, aerodynamics analysis must be performed. It was not founded any study in literature about wheelchair racing aerodynamics analysis by CFD. However, is is possible to find some studies assessing aerodynamics by experimental tests and analytical models. Thus, there is a need to fulfil this lack of research assessing the aerodynamics of a wheelchair racer by CFD. Then, it becomes possible to provide details about pressure, viscosity and total drag, respective drag coefficients, effective surface area and estimate the mechanical power and energy cost to overcome the resistive forces.

1.5. Study aims

This thesis aimed to:

- Review the literature on aerodynamics in wheelchair racing;
- Compare two different helmets (road vs time trial) at several speeds and head positions by CFD.
- Assess the aerodynamics in different key-moments of the stroke cycle by CFD;
- Compare the mechanical power and energy cost of transportation delivered by an elite wheelchair sprinter in key-moments of the stroke cycle.

1.6. Hypotheses

The hypotheses under testing were:

- There is a lack of research in the use of numerical simulations by CFD in wheelchair racing.
- A time trial helmet is more effective compared to a track helmet keeping a neck hyperextension.
- The aerodynamics of a wheelchair racing athlete varies in different phases of the stroke cycle.
- The mechanical power and energy cost in elite wheelchair racing vary in different phases of the stroke cycle.

1.7. Significance of the study

This thesis gave insights about the type of helmet to wear. This may prevent that para-athletes adopt postures and/or positions that can impair the aerodynamics and ultimately their performance. This thesis may help athletes about which garment's wear and body postures and positions adopt during a sprinting event.

Based on the findings reported here, researchers may design, produce and customize helmets for a specific athlete. Advice on the athlete's positions and helmets to be wear can also be provided. Knowing athletes drag, coaches can also estimate the mechanical power and energy cost of the athletes at different positions and speeds. Based on this work, coaches should develop an evidence-based practice basing their sets on a target mechanical power.

1.8. Thesis structure

This thesis is composed by a series of four studies:

- Chapter 2 is a revision of the determinant factors in wheelchair racing sprinting events, technological appliance in this modality and aerodynamic drag evaluation methods.
- Chapter 3 compares the differences between aerodynamic drag in two different positions (looking downwards and forward) with a time-trial helmet at different speeds.
- Chapter 4 compares the variations on the aerodynamics of a world-ranked wheelchair sprinter in the key-moments of the stroke cycle: a numerical simulation analysis.
- Chapter 5 compares an estimation of mechanical power and energy cost in elite wheelchair racing by analytical procedures and numerical simulations.

As last chapter a final discussion will be presented by the presented studies (Chapter 4), followed by the main conclusion and limitations of this study (Chapter 5). Some suggestions for further studies are presented in chapter 6.

Chapter 2. Technologic Appliance and Performance Concerns in Wheelchair Racing – Helping Paralympic Athletes to Excel.

Abstract

Numerical simulations have provided useful evidence in helping several sportsmen to excel in their field. This methodology aims to have a deeper understanding on the influence of equipment and sports techniques on sports performance. In wheelchair racing, technology was used without considering specific sport (some of the Paralympic sports used the same technology of their Olympic counterparts). It has induced unique changes in prosthetic and wheelchair devices. Eventually, technology has become an essential part of Paralympic sports, wheelchair-racing being one of the most popular events. Numerical simulations can help us gather evidence on the effects of drag force acting upon the athlete-chair system.

Different types of wheelchairs are designed for racing (track and road races), net, and invasion sports. One of the various strategies to enhance performance is to minimize the aerodynamic drag of the frame, tires, helmet, sports outfit, and body posture.

Numerical simulations can be used to predict the fluid dynamics.

The goal of this chapter is to review the state-of-the-art numerical simulations and suggest further studies in wheelchair racing. The chapter will include sections covering: (i) main determinants in wheelchair racing; (ii) the effect of aerodynamic force in in wheelchair racing performance; (iii) analytical models, experimental testing, and numerical simulations in wheelchair racing; and (iv) numerical simulations on equipment and techniques.

Keywords: CFD, Paralympic, Performance.

2.1. Introduction

Wheelchair racing it's a major event in Paralympics. In this sport are held races from short (100m) to long distances (42km). The athletes are classified according to their condition into classes (T5i, i.e., i=1, 2, 3 and 4 with injuries at C5-6, C7-8, T1-7 and T8-S4 respectively) (IWAS, 2008; IPC, 2007)]. In wheelchair racing sports science, has been expressed as a need the modelling and computer simulations of racing wheelchairs and the racing itself (Depaux, 1986; Depaux, 1988).

In 1960 took place in Rome, the first games for disabled persons in pair with the Olympic Games. Pioneer research on wheelchair racing happened in the 1980s based on high-speed films at laboratory or running track settings (Cooper, 1990c). In the 1980s, manufacturers estimated that more than 10,000 racing wheelchairs commercialized worldwide (Lakomy, Cambell & Williams, 1987). Being this sport increasingly popular, the competitions became tighter between contenders and research is eagerly needed to help Paralympic athletes to excel.

These days, most world-ranked Paralympic athletes, including wheelchair racers, develop an evidence-based practice with the help of coaches and sports analysts. Every detail of a race is deeply examined to have a deeper insight of the determinant factors that might help to excel. The resistance acting on the wheelchair racer is one of the major concerns for practitioners. The resistance force having an opposite direction to the displacement must be minimized so that for a given amount of thrust, the subject can reach a higher acceleration and speed. Lately a few research projects were reported in the literature under this topic. So, the aim of this chapter is to review the state of the art on the numerical simulations in wheelchair racing and suggest further studies in the sport.

2.1.1. The wheelchair race

The stroke cycle in wheelchair racing is divided in two phases, the propulsion and the recovery phase (figure 1). The propulsion phase is characterized by the tangential force applied to the handrim. In the beginning of the race, these one should be as high as possible and for the longest contact time so that the mechanical impulse is high (Ridgway, Pope & Wilkerson, 1988). Propulsion phase represents 33% to 35% of the full stroke cycle. 65% to 67% of the stroke time is the recovery phase in elite wheelchair racers (Bymes, 1983; Cooper, 1990b; Ridgway, Pope & Wilkerson, 1988; Sanderson & Sommer, 1985). In the recovery phase we have the time period that the hand does not contact the rims. The hand tends to follow different paths until being positioned in the rim again to a new propulsion phase (Cooper, 1990; Davis, Ferrara & Byrnes, 1988; Higs, 1985). However, the recovering phase may change,

the free chosen push frequency (the preferred stroke frequency adopted by each subject) ranged from 32 to 86 pushes/min at a 6.58 m/s in wheelchair racing.

The stroke cycle can also be divided in 5 phases: catch, drive, release, lift and stretch and finally acceleration. Catch is the hand contact moment on the handrim, it usually occurs nearly the 1 and 2 o'clock. Drive phase is the moment of the hand and wrist acceleration on the handrim and it usually occur nearly the 2 and 5 o'clock. Release phase is the moment of the contact breaking of the hand with the handrim, closer to the 6 o'clock. Lift and stretch phase is characterized by the elbow flexion and elevation in the sagittal plan. Acceleration moment is when the elbow extension is done before the handrim contact.

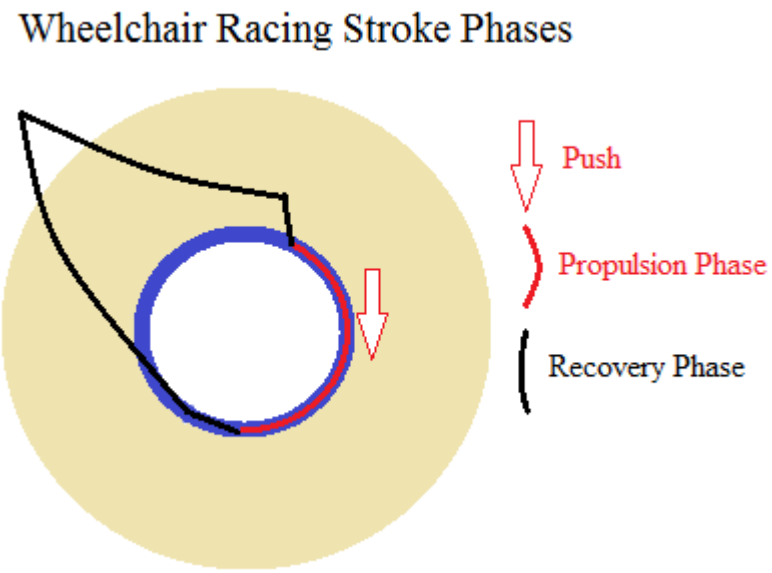

Figure 1. Stroke cycle in wheelchair racing.

During a race, the racers aim to reach the maximal speed as soon as possible and keep it for the remaining time (Figure 2). Figure 2 also depicts the intra-cycle speed (i.e due to hand contact and recovery phase). So, from here this becomes clear that at a given moment propulsive forces are higher than resistance ones (i.e. positive acceleration) and other than the later ones have a higher intensity (i.e. negative acceleration).

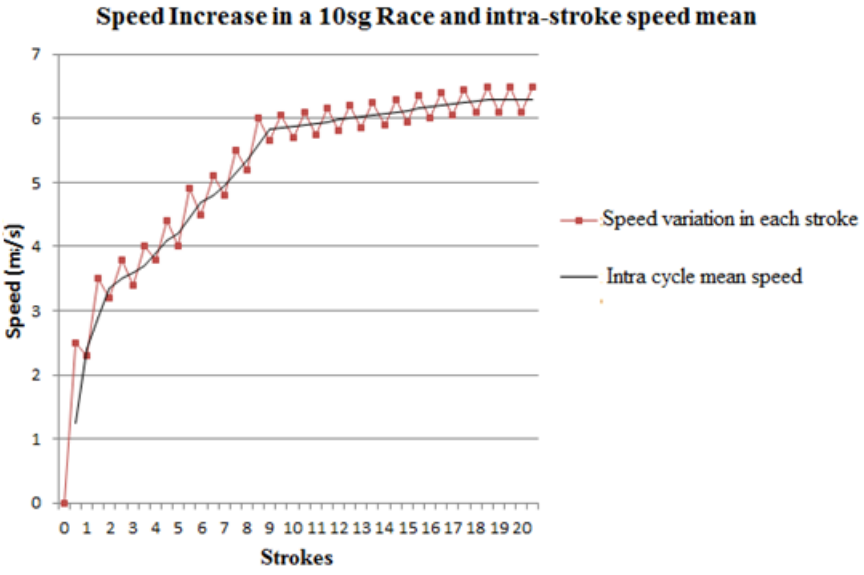

Figure 2. Theoretical representation of the speed over time in 20 stroke cycles.

Stroke kinematics are selected on regular basis to report the stroke cycle. These include the assessment of the average speed, stroke frequency and stroke length.

The stroke frequency can be evaluated by measuring the number of cycles per minute and stroke speed is given by the product of stroke length by the stroke frequency. Stroke length is the difference between the contact distance of a stroke and the contact covered distance of the next stroke. Thus, stroke length can be explained as the covered distance with handrim contact in one stroke (Chow & Chae, 2007). The average speed is calculated dividing the stroke length by the stroke frequency (Chow & Chae, 2007).

A higher stroke frequency combined with the hand linear velocity will lead to a greater energy cost, and probably will enhance cardiorespiratory stress affecting blood lactate and heart rate (Costa et al., 2009). The increase of speed it is related with blood lactate concentration and the rise of heartrate. Despite this, the increase of the handrim diameter seems to reduce the blood lactate concentration at 20km/h, however it didn't happen at 22km/h (Costa et al., 2009).

An increased time of hand contact on the handrim without wrist acceleration will generate deceleration by friction resistance applied by the hand on the handrim. Therefore, to achieve a lower contact it is recommended to produce a high speed soon after the start (O'Connor, Robertson & Cooper, 1998), which is possible to improve as demonstrated by sprinters in strength development (Keogh, 2011). The elbow motion seems to range from 60.9º to 5.2º in flexion to extension movement and the maximum flexion velocity ranges between 515.4º/s and 572.8º/s, which is independent of the light weight of the wheelchair. However, the propulsion arc reduces by 12º to 14º in the pumping-stroke technique, that results from the

shortest handrim contact possible, usually at the start of the race (Rudins et al., 1997). In the 1986 National Wheelchair Track and field Championship in Illinois, in elite finalists, both in paraplegic and quadriplegic wheelchair racers, the mean velocity-time ranged in each stroke from 5.1m/s to 5.5m/s and 3.7m/s to 4.27m/s respectively. The mean velocity in each stroke ranged 0.4m/s and 0.6m/s between the propulsion and recovery phase for the same subjects respectively. As the stroke frequency increases, velocity peak also enhances, despite the negative correlation between the velocity peak and the hand contact time with the handrim. The contact phase of the hand in handrim ranged from 13.58º to 15.6º for quadriplegics and paraplegics. The start acceleration phase at the rims starts at 48.54º and 71.1º. The break contact happens at 187.5º and 238.9º. The peak velocity for each stroke, occur at 181.1º and 223.5º for quadriplegics and paraplegics respectively. These results were founded in a 10 second sprint with 20 to 25 propulsive cycles (strokes) for each subject (Gehlsen, Davis & Bahamonde, 1990).

The velocity peak seems to occur near to the 10 seconds of sprint in wheelchair track racers (Ridgway, Pope & Wilkerson, 1988). Wheelchair basketball players, achieve 80% of the peak velocity in the first three strokes. Otherwise, wheelchair racers at the third stroke only achieve 55% of the peak velocity. The stroke frequency in short distances is greater than in long distances. In 10 seconds, sprints were obtained with 2 strokes per second (Couts, 1990). However, in an 800m race, the stroke frequency ranged between 1.77 and 1.72 Hz (Ridgway, Pope & Wilkerson, 1988).

2.2. Main Determinants in Wheelchair Racing

The wheelchair racing athlete intends to reach the maximum acceleration as soon as possible. According to Newton's second law the acceleration (a) in given as the ratio between force (f) and mass (m) (Equation 1).

$$a = \frac{F}{m} \quad (1)$$

In the wheelchair racing case, it is also possible to say that,

$$a = \frac{(F_{Prop} - F_{Resist})}{m} \quad (2)$$

Where, F_{Prop} and F_{Resist}, are the propulsive forces and the resistive ones respectively.

Positive acceleration is obtained by the applied propulsive forces on the wheels, overcoming the resistive ones (Figure 3). In wheelchair racing the propulsive force is the push on the

handrim, generating motion (i.e. the applied force by the ground in the wheel). The resistive forces are the rolling friction (Fr) and aerodynamic drag (Fd).

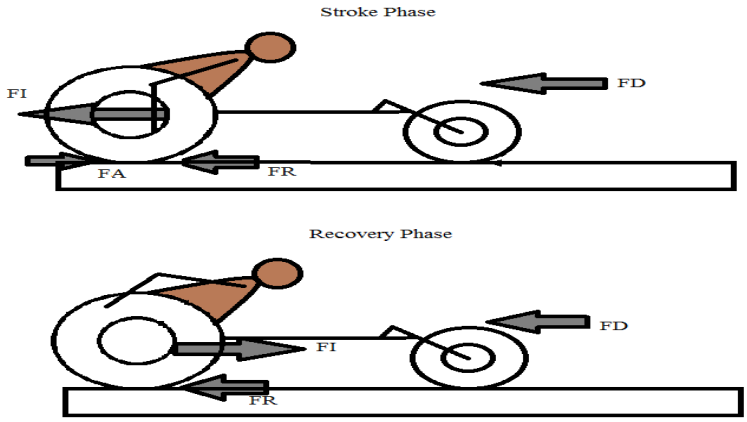

Figure 3. Free body diagram in wheelchair racing [21]; FI – Inertial force; FD – Drag force; FR – Rolling friction forces; FA – The applied force by the ground on the rear wheels.

Fuss (2009) reported an analytical model to describe the performance based on these major determinants. The inertial force is the required force to change the body state and start the motion. The drag force is the air resistance to the wheelchair-athlete system. Rolling friction is the resistive force of the ground on the wheels' tires. Considering Newton's third law, the applied force by the ground on the rear wheel is the opposite one of the wheel in the ground derived by propulsion.

According to Fuss (2009), the total energy expended by the athlete is taken by rolling friction and air drag. It is possible to say, that the velocity is dependent on the kinetic energy of the system, and mass.

$$v = \sqrt{\frac{2(E_{in} - E_{loss})}{m}} \quad (3)$$

In the equation, v is the velocity, E_{in} is the energy produced by the athlete and E_{loss} is the energy lost.

$$E_{kin} = E_{input} - (E_{drag} + E_{friction}) \quad (4)$$

The total kinetic energy is obtained from the sum of all mobile parts with a speed higher than zero. It is also considered that other movement oscillations do not contribute to the kinetic energy. Then:

$$E_{kin} = \frac{mv^2 + \sum_{i=1}^{3} I_i \omega_i}{2} \quad (5)$$

In equation 5, Ii is the moment of inertia and ωi is the angular velocity of wheel i.

When the inertia force (FI) gets combined with distance, the kinetic energy (Ekin) can be formulated as:

$$E_{kin} = \int_{x1}^{x2} F_I \, d_x \quad (6)$$

Equations 7 and 8 consider that velocity comes from the work of the rear wheel (ωri) and acceleration is the angular velocity of the rear wheel (a = αri), then solving it for FI, we obtain:

$$F_I = a\left(m + \sum_{i=1}^{3} \frac{I_i}{r_i^2}\right) \quad (7)$$

In this formula, m is the mass of wheelchair-athlete system and I is obtained from the relation between the one wheel mass and the wheel radius gyration squared. The mass of one wheel times its radius of gyration squared. When accelerated, an equivalent mass results in FI:

$$M = m + \sum_{i=1}^{3} \frac{I_i}{r_i^2} \quad (8)$$

The propulsion cycle is given by the stroke and recovery phases, the equilibrium forces in the stroke one are given by:

$$F_A + F_I + F_D + F_R = 0, \quad (9)$$

$$F_A + M_a + C_{Dv^2} + mg\mu_R + mgk_{fv^2} = 0 \quad (10)$$

CD is the drag coefficient, v is the instantaneous velocity (considering distance and time at a given moment) and the acceleration ($d^2x/\ dt^2$). The CD cluster is obtained from, 0.5ρcDA, being the product of air density (ρ) with the drag coefficient of the air (C_D) and the frontal surface area (A). Considering that wheelchairs are in straight line and according to Equation 14, 12 and 13, FR is given by:

$$F_R = \mu_R mg + k_f mgv^2 \quad (11)$$

Where μ_R is the rolling friction coefficient, m is the mass, g the gravitational acceleration and k_f the coefficient of speed.

$$F_A + M_a + c_1 v^2 + c_2 = 0 \quad (12)$$

C_1 is given by,

$$c_1 = C_D + mgk_f \quad (13)$$

And C2,

$$c_2 = mg\mu_R \quad (14)$$

Thereby, in a wheelchair-athlete system the responsible variables for the energy losses are FD and FR and both forces are equal to zero in a loss-free environment.

2.2.1. Propulsion

In the propulsion phase, Fuss (2009) described 4 forces as the main ones. The ground applied one at the rear wheel, aerodynamic drag force and the rolling friction one. When the mass gets accelerated produces an inertial force (FI). The kinetic energy derived from FI, is stored on the wheels, it depends of the moment of inertia and the angular speed of the wheels creating the system motion. The 4 forces in equilibrium are described as,

$$F_A + F_I + F_D + F_R = 0 \quad (15)$$

F_A Is the force applied to the ground on the wheels derived from the tangential force applied on the handrim (F_I). For movement occurring, F_A must be higher than F_I, F_D and F_R.

Several investigations have been made to better understand the physiological factors and demands that may affect the wheelchair propulsion. Others for instance, (Sanderson & Sommer, 1985) presented the motion of the racing wheelchair derived by the sum of all external forces by:

$$F(R/r_{pr}) = My + Iv/R + I_f\, v/r + Fa + M_B/r_{ax} + M_b/r_{axf} + F_R + F_r + Wsin0(x) \quad (16)$$

Where, "R/r_{pr}" represents the gear ratio of the handring to the wheel. F - The tangential force in the handrings; R and r_{pr} - The radius of the rear wheels and handrings; M - The mass of the system athlete-wheelchair; v - The velocity of the athlete-wheelchair system, given by: v = x = dx/dt; I and I_f- The inertia of the rear wheels and the wheels inertia; r - The radius of the front wheels; Fa - The air resistance of the athlete-wheelchair system; M_B - The rear hubs bearing resistance; M_b - The front hubs bearing resistance; r_{ax} and r_{axf} - The radius of the rear and front axles respectively; F_R and Fr- The rolling resistance of the rear and front wheels respectively; W - The weight of the athlete-wheelchair system; Θ (x) - The inclination angle (i .e., changes in elevation); x - The covered distance;

2.2.2. Inertia

The sum of the kinetic energy to all mobile parts is given by equation 5. that includes the energy of the 3 wheels and the translational energy. The kinetic energy is equal to the inertial force combined with distance (equation 6). Thus, the inertial force (F_I) is given by:

$$F_I = aM \tag{17}$$

M represents the sum of the inertial moments.

The Inertial Force is the required force for a body state change. At the beginning of the wheelchair race, the inertial force is the required force for starting the wheelchair. Therefore, it is clear that the mass influences the inertial moment in the system and that the mass reduction will lead to a sooner and/or higher speed. Fuss (2009) reported that a reduction of 1kg in a wheelchair-athlete system will improve the winning time by 0.132sg.

2.2.3. Air Drag and Rolling Resistance

In wheelchair racing, the air drag results from the air resistance in the surface area of the athlete-wheelchair system. In contrast, the rolling resistance results from the friction of the tyres on the ground. Aerodynamic resistance can be minimized by reducing the frontal area of the subject, intending to improve the winning time of a racing wheelchair. At speeds greater than 5m/s aerodynamic drag represents 90% of the resistive forces (LaMere & Labanowich, 1984). Between 5.32m/s and 6.83m/s, rolling resistance is greater than aerodynamic drag with a partial contribution of 65% to 75% and 25% to 35% respectively. At greater speeds, aerodynamic drag starts to represent a greater contribution of the resistive forces (Barbosa, Forte, Morais & Coelho, 2014).

Air drag and rolling resistance can be acceded from equation 18 for rolling resistance and equation 19 for air drag:

$$F_R = \mu_g mg + k_f mgv^2 \tag{18}$$

$$F_D = 0.5\rho A_d v^2 C_D \tag{19}$$

In these two equations, F_R is the rolling friction, μ_g is the rolling friction coefficient, m is the mass of the athlete-wheelchair system, g is the gravity acceleration and k_f is the coefficient of the speed influence in rolling resistance force, ρ is the air density, A_d is the frontal area, v^2 is the velocity and C_D is the drag coefficient.

Lightweight clothes worn by wheelchair racers to reduce the aerodynamic drag (Barbosa, Forte, Morais & Coelho, 2014). A flexed upper trunk position also reduces the aerodynamic drag, as does reducing the rear wheel spokes to 24 (LaMere & Labanowich, 1984). In cycling, a flexed upper trunk position reduces the frontal area in 20% to 29% (Burke, 1986). In wheelchair racing, the same position reduces the frontal area in 3% to 4% (Hedrick, Wang, Moeinzadeh & Adrian, 1990).

Mass would also influence the rolling friction; reducing the wheelchair-athlete system would also improve the speed, mainly in short distances. A 1kg reduction would improve 1-2.3% of the winning time in wheelchair racing (Fuss, 2009).

2.3. Analytical Models, Experimental Testing and Numerical Simulations in Wheelchair Racing

2.3.1. Experimental testing: Coast-down Technic

Aerodynamic and rolling resistance can be tested providing realistic opportunities that cannot be achieved in laboratory. The coast down-methods founded in literature are: (i) - roll distance applying the ramp methods; (ii) – the timing gate method, that measures the velocity decrease in different points between two marks (gates); (iii) – The velocity method that measures directly the speed in each time.

The roll distance applying the ramp method consists rolling, a wheelchair from a ramp to the field, measuring the covered distance by the wheelchair (FIFA, 2001). The timing gate method was developed as an alternative to the roll distance, produced in less time and space compared with the whole roll until the wheelchair stops. Two marks should be performed counting the time when the wheelchair passes between them (Kolitzus, 2003). In the velocity method, the racer reaches the maximum speed, stops the propulsion and the velocity is recorded in each instant (Kolitzus, 2003; Fuss, 2009). A dynamometer-based coast-down test was used for the wheel deceleration calculus (Kwarciak, Yarossi, Ramanujam, Dyson-Hudson & Sisto, 2009). For wheel deceleration in each trial, hub (Hub_{xyz}) and handrim (Rim_{xyz}) markers were placed. The wheel rotation on each time was assessed by the law of cosines:

$$\theta = \cos^{-1}\left(\frac{A \times B}{\|A\|\|B\|}\right) \quad (20)$$

A = Rimxyz(i) – Hubxyz(i); B = Rimxyz (i + 1) – Hubxyz (i + 1).

To avoid wheel size differences, the angular speed was converted in linear one. It was fitted a line to the linear velocity (v) data intending to determine the wheel deceleration (ad), the time to coast down from 2 m/s to 1 m/s is represented by "t" and the initial wheel velocity is represented by "v_0".

$$v = a_d t + v_0 \tag{21}$$

The estimation for rolling resistance can be done based on Cooper's method (Sanderson & Sommer, 1985). Intending to simplify the method, aerodynamic drag, wheel and roller bearing resistances, as other external resistances were neglected. Thus, the rear wheel motion was described by:

$$T_w = \left(I_r \frac{R}{r} I_w\right) a_w + F_{RR} R \tag{22}$$

Where, "Tw" was the torque applied by the hand to the rear wheel; "Ir" and "Iw" were the moment of inertia of the roller and the rear wheel, respectively; "r" and "R", the roller and rear wheel radius, respectively; "aw" and "FRR" as the angular acceleration of the rear wheel and the rolling resistance force respectively.

Considering that the propulsive force was discontinued, "Tw" is equal to zero, and "aw" represents the wheel angular deceleration. The equation is being used to describe the rear wheel rotation. The roller inertial moments (0.87 ± 0.15 kg-m^2) and wheels (0.12 ± 0.02 kg-m^2) were experimentally acceded resourcing the acceleration method by DiGiovine et al. (2009). Applying the "Ir" and "r" values into Equation 22, and rewriting "aw" as the ratio between linear deceleration and radius (ad/R), rolling resistance force is obtained from the wheel radius, inertia, and deceleration, calculated by:

$$F_{RR} = \frac{-a_d}{R^2}(I_w + 5.47R) \tag{23}$$

Coast-down distance (CDD) calculation was computed using the equation of motion, where acceleration is assumed to be constant and t is the time for coast-down technic ends, when the wheelchair stops:

$$CDD = \frac{1}{2} a_d t^2 + v_0 t \tag{24}$$

Another method consists in accelerating the wheelchair (e.g., from 2.5 to 12.8m/s). The rider stops the propulsive phases reaching the target speed counting the length and/or time until the wheelchair stops (Candau et al., 2001). In this method both aerodynamic drag and rolling resistance are obtained. The figure 4 depicts a speed decay of wheelchair considering the velocity method, measuring the speed in each time.

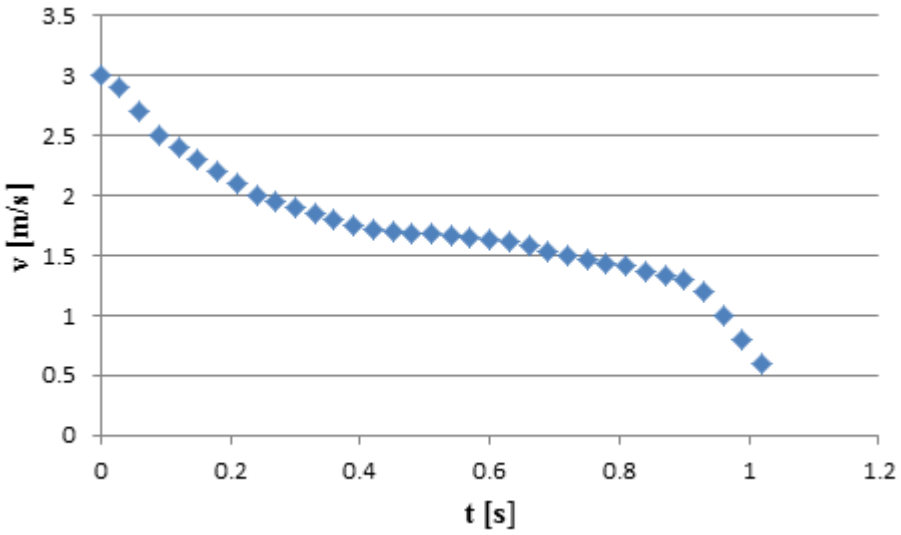

Figure 4. The velocity decay of a manual wheelchair over a typical trial.

2.3.2. Wind tunnel testing

At least one paper can be found in the literature reporting the assessment of the aerodynamics in wind tunnel between two wheelchair models (MacLeish, Cooper, Harralson & Ster, 1993). The drag forces were measured for speeds between 54.86km/h and 164.60km/h with intervals of 18.28km/h. However, air viscosity and ground motion effect are not taken into account with this methodology. Besides this, a better wind tunnel test should be performed intending to determine the best helmet and clothes to use in races (MacLeish, Cooper, Harralson & Ster, 1993). The Drag was proportional with the speed in the two models A and B. Model A presented a strict nose, with fenders at the wheels and an exceeded front angle attack. The drag force was acceded in grams (gr) and ranged from 26(gr) to 360(gr) in booth models, with and without pilot. With and without pilot, the model B presented a lower drag force for velocities lower than 91.44km/h. At higher speeds the model A presented lower drag force with and without pilot.

From this experimental test it is possible to confirm that specific wheelchairs should be made for specific racers, and a sprint race wheelchair should be different to a long race wheelchair.

2.3.3. Analytical method for drag assessment

For rolling friction and aerodynamic drag, Burton, Fuss & Subic (Burton, Fuss & Subic, 2010) presented an analytical procedure to estimate rolling friction and aerodynamic drag. FR is non-linear when calculated from visco-elastic models, considering the deformation of the

tyres, reduces in the ground higher speed in parabolic function. The equations for these two forces are expressed before in equations 18 and 19.

According to Fuss (2009), based in vehicles data (Petrushov, 1998), considering that the μ_g of a racing wheelchair is 0.01, K_f is $5x10^{-6}$ s^2m^{-2}, a mean speed of 10 m/s and a mass athlete-wheelchair system of 80kg the first and second term of the equation 22 is 7.85 and 0.35N.

In a partial contribution assessment of air drag, Barbosa et al., (2014) assumed the air density of 1.2041 kg/m3 in the sea level at 20° C. The surface area was measured with the photogrammetric technique in the frontal plane and the drag coefficient was assumed to be 0.7. All estimations were completed in each speed moment between 0 m/s and 13m/s increasing in every 0.1m/s. considering the world speed record, the air drag represents 34.89%.

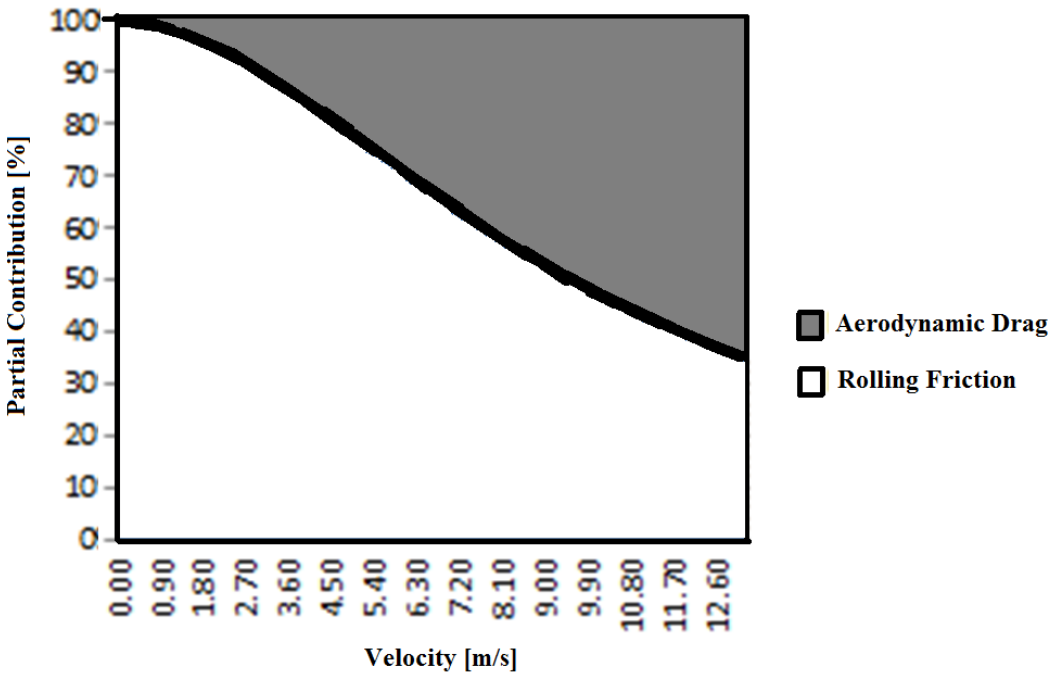

Figure 5. Partial Contribution of aerodynamic drag and rolling friction by Barbosa et al. [23].

2.3.4. Numerical simulations: Computer Fluid Dynamics

Computational Fluid Dynamics (CFD) has been used over the last 20 years. There are a lot of benefits on CFD and tools such as FLUENT, CFX, STAR-CD and FiDAP are all commercially available and used in industrial settings in the engineering community since the 1990s. Engineers and scientists started to use these simulations in competitive sports to reach a performance advantage, to improve sports equipment design and elite athletes' aerodynamics or hydrodynamic enhancements (Hanna, 2012).

In sport sciences, the CFD presented concordance between numerical simulations and in vivo tests. For the simulation, a 3D body model scan is required and the images processing can be made with recourse to Anatomics Pro (Anatomics, Kannapolis, NC, USA) and FreeForm (Sensable Technologies, Woburn, MA, USA). The scan files are saved as IGES (*.igs) format, intending to be executable in Gambit/Fluent (Fluent Inc, Hanover, NH, USA). In Gambit/Fluent it is possible generate the greed and to define the finite elements in 3D areas.

The numerical simulation consists in discretization of Navier-Stokes equations by the finites volumes methods. These equations come from Newton's second law in fluid mechanics, assuming that the fluid stress is the sum of diffusion of its viscosity, resulting from an applied pressure term. The equation resolution determines the fluid speed in a determined point at space and time. CFD is based in an approximated finite volume. In this approximation space is divided in small cells to form a mesh or greed, applying a solver algorithm for the equations of fluid volume motion resolution (Marinho, Barbosa, Mantha, Rouboa & Silva, 2012; Marinho et al., 2011).

The Reynolds-Averaged Navier-Stokes (RANS) comes from decomposing the instantaneous values into means and/or fluctuating components. Fluid flow behaviour (equation 25), Reynolds Stresses (equation 26), temperature (equation 27) and mass transfer (equation 28) can be solved in this methodology.

$$\frac{\partial \mathrm{Ui}}{\partial \mathrm{xi}} = 0 \tag{25}$$

$$\frac{\partial_{Ui}}{\partial_t} \pm U_j \frac{\partial_{Ui}}{\partial_{x_j}} = -\frac{1}{\rho}\frac{\partial P}{\partial x_j} + \frac{\partial}{\partial x_j}\left(2vS_{ij} - \overline{\mu_j{}'\mu_i{}'}\right) \tag{26}$$

$$\frac{\partial_{\theta i}}{\partial_t} \pm U_j \frac{\partial_\theta}{\partial_{x_j}} = \frac{1}{\rho_{cp}}\frac{\partial}{\partial x_j}\left(k\frac{\partial \theta}{\partial x_j} - \overline{\mu_j{}'\theta'}\right) \tag{27}$$

$$\frac{\partial_C}{\partial_t} \pm U_j \frac{\partial_C}{\partial_{x_j}} = \frac{\partial}{\partial x_j}\left(D\frac{\partial C}{\partial x_j} - \overline{\mu_j{}'c'}\right) \tag{28}$$

The μ_i and x_i are the instantaneous velocity and the position, p the instantaneous pressure, t is the time, ρ the fluid density, υ is the molecular kinematic viscosity, c_p heat capacity, k the thermal conductivity and S_{ij} the strain-rate tensor, c is the instantaneous concentration and D the molecular diffusion coefficient.

The Reynolds stresses component ($\overline{\mu_j{}'\mu_i{}'}$), describes the turbulence of the mean flow being the exchange of momentum by the change of the fluid parcels. In a laminar flow, the molecules are the responsible for momentum exchange (molecular viscosity). However, in a turbulent flow (turbulent viscosity) the parcels of flow are the ones that exchange the

momentum. To finish this calculus, it is also necessary to use a turbulence model to represent flow scales. The first order Boussinessq eddy-viscosity hypothesis to model the Reynolds stress in function of velocity and time is used. However, it is also a necessary model for the linear or non-linear eddy-viscosity distinction. The Reynolds stress is given by:

$$\overline{\mu_j{}'\mu_i{}'} = 2v_t S_{ij} - \frac{2}{3}k\delta_{ij} \tag{29}$$

Where, v_t is the turbulent viscosity and the mean strain rate S_{ij} is given by,

$$S_{ij} = \frac{1}{2}\left(\frac{\partial U_i}{\partial_{xj}} + \frac{\partial j}{\partial_{xi}}\right) \tag{30}$$

The turbulent kinetic energy (k) is given by,

$$k = \frac{1}{2}\overline{\mu_i{}'\mu_i{}'} \tag{31}$$

And the kronecker delta (δ_{ij}),

$$\delta_{ij} = \begin{cases} 1; \; if \; i = j \\ 0; if \; i \neq j \end{cases} \tag{32}$$

Assuming the gradient diffusion (Gradient-diffusion Assumption) for heat and mass fluxes, as function of the temperature gradients in the mean flow, the turbulence hot flow is given by,

$$-\overline{\mu_j'\theta'} = D_{\theta t}\frac{\partial \vartheta}{\partial_{xi}} \tag{33}$$

Where $D_{\theta t}$ is the turbulent heat diffusivity (turbulent Prandtl number), and $\frac{\partial \vartheta}{\partial_{xi}}$ is the temperature gradient in the mean flow. The turbulent Prandtl number is obtained by,

$$Pr_t = \frac{v_t}{D_{\theta,t}} \tag{34}$$

And the turbulent mass flow $-\overline{\mu_j' c'}$ is given by,

$$-\overline{\mu_j' c'} = D_{c,t}\frac{\partial C}{\partial x_i} \tag{35}$$

Where, $D_{c,t}$ is the turbulent mass diffusivity (turbulent Schmidt number) and $\frac{\partial C}{\partial x_i}$ the concentrated gradient in the mean flow. The turbulent Schmidt number is calculated from equation 36,

$$Sc_t = \frac{v_t}{D_{\theta,t}} \quad (36)$$

Once RANS needed a turbulence model, less expensive equations are created with additional variables, transforming in meanings of the instantaneous equations calculations. This results from removing several small equations and adding other unknown variables, determined by the turbulence models. Standard K – ε turbulence model was used by Caboz (2010) in a computational simulation on a counter-clock cyclist helmet, however it is only valid in a completely turbulent fluid. The same mode is assumed for wheelchair racing. In Fluent the turbulence models available are: (i) Standard K – psilon; (ii) Standard K – ε; (iii) Spalart – Allmoras; (iv) Reynolds Stress (RSM) (White, 1999).

In this model (Standard K – ε) the Bussinesq hypothesis is given by,

$$-\rho\overline{\mu_i'\mu_j'} = 2\mu_t S_{ij} - \frac{2}{3}\rho k\delta_{ij} \quad (37)$$

Where the turbulent viscosity,

$$\mu_t = \rho C_\mu \frac{k^2}{\varepsilon} \quad (38)$$

The mean tension rate is given by the equation 30. The kinetic energy of turbulent fluctuation and the dissipation of the kinetic energy (m^2/s^2) are given by equations 31 and 40 respectively.

$$k = \frac{1}{2}\overline{\mu_i'\mu_i'} = \frac{1}{2}\overline{\mu'^2} + \overline{v'^2} + \overline{w'^2} \quad (39)$$

k, is the energy measuring associated with the turbulent fluctuations in the flow.

$$\varepsilon = v\frac{\overline{\partial\mu'_i\partial\mu'_i}}{\partial x_j\partial x_j} \quad (40)$$

ε, is caused by the work of the smallest eddies against the viscous stresses in the flow.

Then the determination of k (equation 41) and ε (equation 42) by their transport equations are,

$$\rho\frac{\partial k}{\partial t} + \rho\frac{\partial}{\partial x_i}(k\mu_i) = \frac{\partial}{\partial x_j}\left(\left(\mu + \frac{\mu_t}{\sigma_k}\right)\frac{\partial k}{\partial x_j}\right) + G_k + G_b - \rho\varepsilon \quad (41)$$

$$\rho\frac{\partial \varepsilon}{\partial t} + \rho\frac{\partial}{\partial x_i}(\epsilon\mu_i) = \frac{\partial}{\partial x_j}\left(\left(\mu + \frac{\mu_t}{\sigma_\varepsilon}\right)\frac{\partial \varepsilon}{\partial x_j}\right) + C_{1\varepsilon}\frac{\varepsilon}{k}(G_k + C_{3\varepsilon}G_b) - \rho C_{2\varepsilon}\frac{\varepsilon^2}{k} \quad (42)$$

Where, $\rho\frac{\partial\varepsilon}{\partial t}$ and $\rho\frac{\partial k}{\partial t}$ are the variation of the local in time, $\rho\frac{\partial}{\partial x_i}(k\mu_i)$ and $\rho\frac{\partial}{\partial x_i}(\epsilon\mu_i)$ the adjective term, $\frac{\partial}{\partial x_j}\left(\left(\mu+\frac{\mu_t}{\sigma_k}\right)\frac{\partial k}{\partial x_j}\right)$ and $\frac{\partial}{\partial x_j}\left(\left(\mu+\frac{\mu_t}{\sigma_\varepsilon}\right)\frac{\partial\varepsilon}{\partial x_j}\right)$ are the diffusion, G_k is the generation of k by the gradients mean velocity, G_b the generation of k due the fluctuation and ρε the dissipation of k. σk and σε are the turbulent Prandtl numbers for k and ε respectively. And the constants $C_{1\varepsilon}$, $C_{2\varepsilon}$, C_μ, σ_k e σ_ε were experimentally determined, $C_{1\varepsilon}$ = 1.44; $C_{2\varepsilon}$ = 1.92; C_μ = 0.09; σ_k =1.0; σ_ε = 1.3.

The Gambit software allows the building of a representative graphic model of the volume subdivided in sub volumes, trying to make the process as realistic as possible. This software also allows defining the frontiers. In solid frontiers and close to them, the FLUENT software computes the Reynolds tension and ε. It applies solid specific frontiers conditions for Reynolds tension using balance hypotheses, without considering the convection and diffusion of tension transport (equation 25). In a local coordinate system, T is tangential coordinate, η the normal and λ the binomial one. The Reynolds tension in the adjacent cells to the frontier, are calculated by the equation:

$$\frac{\overline{\mu'^2_t}}{k}=1.098,\frac{\overline{\mu'^2_\eta}}{k}=0.247,\frac{\overline{\mu'^2_\lambda}}{k}=0.655,\frac{\overline{\mu'_t\mu'_\eta}}{k}=0.255 \quad (42)$$

FLUENT solves the transport equation (41) for k obtaining. For calculous convenience the equation is globally solved, albeit the calculus of the k values is only necessary near the frontier. In the rest of the domain the k is calculated by the equation (26).

The mesh can be constructed by quadrangular elements, with a space size of 0.1mm. The resulting data from the computational simulation of the determined flow regime and the visualisation of the pressure profiles and speed are obtained by FLUENT. The data's processing allows calculating the drag coefficient in the diverse forms (Carvalho, 2008).

2.3.5. Numerical Simulations on Wheelchair Racing

CFD methodology starts being used for equipment tests. In wheeler riders' helmets, CFD has shown that airflow velocities could be improved with grooves in polymer foam liner and also improving the sweat evaporation. A top helmet hole would improve the velocity in that point, however velocities at the back became lower (Pinnoji & Mahajan, 2006).

The ideal posture and some changes in the wheelchair could be possible to define the three first places. The tests revealed that the most drag negative influence in performance came from the athlete and not from the wheelchair. With a subtle modification in the seating position it could save 10% of the aerodynamic drag. No results were presented by the authors relatively to the wind tunnel test (Rushby-Smith & Douglas, 2012).

CFD methodology must be applied in different fabrics, helmets and wheelchairs. The frame design, as the tube sizes must influence the fluid flow behaviour. Also different positions should be considered to be analysed the flexed head in the start of the race or the look forward position. In each stroke phase, the different fluid flows should also be analysed intending to reach the ideal motion in the stroke phase and recovery one, as the effect of the wheelchair designs and materials in the fluid flow (Barbosa, Forte, Morais & Coelho, 2014).

Thus, fluid dynamics analysis should be performed intending to evaluate possible different designs of the wheelchairs and fulfil the lack of literature in this area. There is a need of results presentation such as drag and drag coefficient in different positions, helmets and cloths at different speeds.

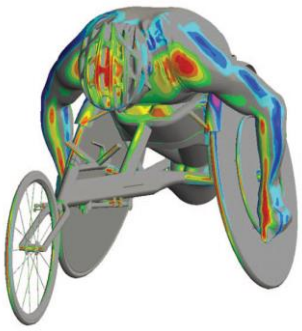

Figure 6. CFD methodology of a scanned model in TotalSim (http://www.totalsimulation.co.uk/wp/cfd-image-gallery/)

2.4. Summary and Conclusions

The sports science of wheelchair racing lacks research. However, there is some information that could positively contribute to increase performance in athletes. Managing the mathematical models based on physics laws, coaches could identify the mechanic performance obstacles and try to minimize them.

The drag reduction by the rolling and air resistance assess also contributed to increase the performance in athletes. Better propulsion could be obtained by reducing the total drag combined with a mass reduction and other possible aerodynamic positions. The purpose of computational simulations and/or computer fluid dynamics is the time improvement achieved by reducing the aerodynamic drag. No data was found about CFD tests in wheelchair racing.

The stroke technique should also be focused. Despite that there are no indications about how many hours that should be taken off training after an injury occurrence. It is defined that the high angular velocities near the shoulder and the elbow generated by the strokes, induce an

overuse stress increasing the risk for joint injuries. There are also some indications about the contact zones, force applying and contact break at the rear wheels.

Physiological variables should also be studied in wheelchair racing athletes, an area that also has a lack of information in this sport. Thus, a precise control of the total drag and the efficiency of the stroke technique, which is related to high levels of strength derived by the strength and physical condition training, will positively contribute for a better performance.

Chapter 3. Comparison by computer fluid dynamics of the drag force acting upon two helmets for wheelchair racers.

Abstract

The aim of this study was to compare the drag force created by two helmets (time trial and track) used by a wheelchair racer. The head and helmet of the racer were scanned to obtain the 3D models. Numerical simulation was run on Fluent, having as output the drag force for both helmets (track and time trial) in two different positions (0º and 90º) and increasing velocities (from 2.0 to 6.5 m/s). The greatest aerodynamic drag was noted wearing a time trial helmet in 90º ranging from 0.1025N to 0.8475N; this was also the position with the highest drag. The velocity with higher drag for booth helmets was at 6.5 m/s. The time trial helmet at 0º had the lower aerodynamic drag, compared with the same position of track helmet. The drag force seems to be lower wearing the time trial helmet and keeping the 0º position and, thus, should be considered for sprinting events.

Keywords: Helmets, CFD, Wheelchair Racing, Drag.

3.1. Introduction

Computer Fluid Dynamics (CFD) is an area under Computer-Aided Engineering and provide insights on 2D and 3D digital geometries. This methodology has been applied to assess competitive sports such as cycling, swimming, golf or ski jumping. It also allows to assess variables such as drag force, drag coefficient and pressure, of gears, equipment and apparel in these sports (Martin, 2009).

Aerodynamics plays an imports role in sprinting events. It represents more than 90% of the resistive forces at speeds higher than 5m/s (LaMere and Labanowich, 1984). This analysis was done as well at greater speeds, such as 15m/s, 20m/s or even higher (Alam et al., 2014). In sports like cycling, the rider's posture could be evaluated. Small variations in the rider's position could account for 10% variation in the drag force (Rushby-Smith and Douglas, 2012). Being based on the same rational, the helmet used and the position of a wheelchair racer may have a meaningful effect on the resistance, notably in racing sprinting events.

CFD presents concordance between the numerical simulations and experimental testing. A 3D model obtained with specific 3D scan is needed for the computer simulations. Software's such as Artec Studio 0.7 (Artec, USA), Geomagic (3D Systems, USA) and Maya (Autodesk Inc., USA) allows model digitalization, and scans merge and editing. Upon merging the scans and editing, it is possible to generate a 3D mesh, and areas and elements definition (Forte et al., 2015).

This methodology consists in the discretization of Navier-Stokes equations by the finite volumes methods. This set of equations encompass the Newton's second law of motion. The fluid stress, resulted from an applied pressure term and it comes from the sum of diffusion of its viscosity. Reynolds-Avereged Navier-Stokes equations decompose instantaneous values into means and/or fluctuation compounds (Marinho et al., 2011; Marinho et al., 2012). The fluid flow behaviour (equation 1), Reynolds stress (equation 2), temperature (equation 3) and mass transfer (equation 4) could be solved with resource to this methodology.

$$\frac{\partial_{\mathrm{Ui}}}{\partial_{\mathrm{xi}}} = 0 \tag{1}$$

$$\frac{\partial_{Ui}}{\partial_t} \pm U_j \frac{\partial_{Ui}}{\partial_{x_j}} = -\frac{1}{\rho}\frac{\partial P}{\partial x_j} + \frac{\partial}{\partial x_j}\left(2\nu S_{ij} - \overline{\mu_j{}'\mu_i{}'}\right) \tag{2}$$

$$\frac{\partial_{\theta i}}{\partial_t} \pm U_j \frac{\partial_{\theta}}{\partial_{x_j}} = \frac{1}{\rho_{cp}}\frac{\partial}{\partial x_j}\left(k\frac{\partial \theta}{\partial x_j} - \overline{\mu_j{}'\theta'}\right) \tag{3}$$

$$\frac{\partial_C}{\partial_t} \pm U_j \frac{\partial_C}{\partial_{x_j}} = \frac{\partial}{\partial x_j}\left(D\frac{\partial C}{\partial x_j} - \overline{\mu_j{}'c'}\right) \tag{4}$$

Therefore, this technique can be used to learn the effects of different helmets and positions by the wheelchair racer, as the racer can wear either a track helmet or a time trial helmet. It is unclear which model will impose a lower aerodynamic drag. Thus, the aim of this study is to compare two different helmets (track vs time trial) at different speeds and head positions by CFD.

3.2. Methods

A Paralympic wheelchair racer (category T-52) was recruited for this research. He is a European medallist in sprinting events and a world championships finalist. The subject wore two different models of helmets. One is a track helmet (LAS, Istron) and the other a time trial model (LAS, Cronometro).

The geometries were obtained by a 3D scan Artec (Artec-L, Artec Group, Inc., USA). The scans were performed by Artec Studio 0.7 (Artec, USA) (Figure 1).

Fluent (Fluent, Inc., USA, New York) code, allows to compute numerical simulations applying a mathematical model to the fluid flow, at a created domain with discretized algebraic expressions of the Navier-Stokes equations. Fluent software solves the equations with a finite volume approach (Marinho et al., 2011). The domain is represented by a 3D mesh of subdivided cells representing the fluid flow around the head and helmets in the different positions.

Realizable k-epsilon was the applied turbulence model, this one, is much more efficient in computation economy and converged after 1404 interactions (Aroussi et al., 2001).

The 3D mesh was made with more than 6 million cells for booth helmets domains. The angles of attack were set as 0º (i.e., looking forward, with the opposite direction of the fluid flow) and 90º (looking downwards, perpendicular to the fluid flow direction).

The fluid flow velocity was set in inlet portion of the dome surface at 2m/s, with increments of 1.5 m/s up to 6.5 m/s. Typically the wheelchair racer will reach these range of speed over an event. The aerodynamic drag was computed as:

$$F_D = 0.5\rho A_d v^2 C_D \quad (5)$$

Where FD is the drag force, CD represents the drag coefficient, v the velocity, Ad surface area and ρ is the air density (Sanders, 1999).

3.3. Results

The contours of static pressure obtained in fluent, represents the pressure zones (Pa) in the helmets at 6.5m/s. Zones with red colour indicate high pressure and low pressure with blue colour (figure 1). It is possible to observe that the helmet at 90º increases the surface area and consequently the pressure zones.

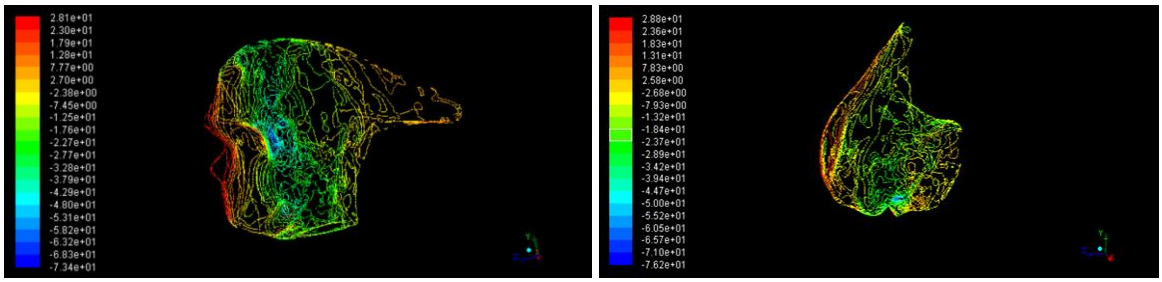

(a) (b)

Figure 1. Static pressure zones of the time-trial helmet at 0º (a) and 90º (b) position, at 6.5 m/s.

It is also possible to recreate the fluid flow velocity simulation around the object at 6.5 m/s. With this simulation it is possible to observe the velocity vectors coloured with the static pressure around the surface area of the geometry (figure 2).

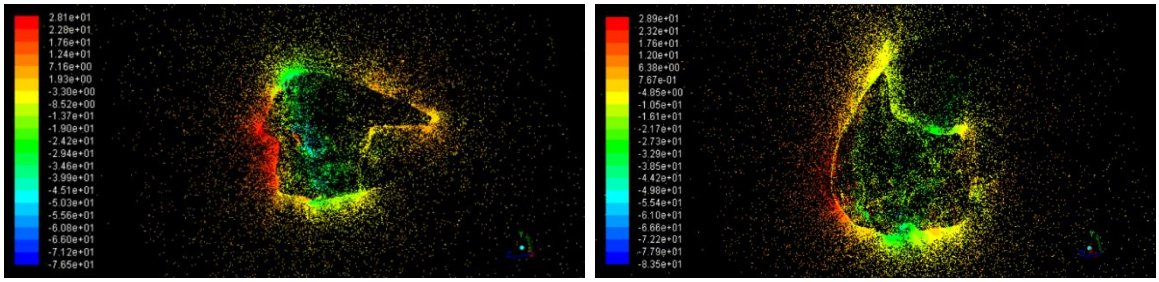

(a) (b)

Figure 2. Flow velocity vectors at 6.5 m/s colored by static pressure on the surface area in time-trial helmet at 0º (a) and 90º position (b) respectively.

Aerodynamic drag is prone to increase for booth helmets with increasing velocities. The drag force ranged between 0.0660 N and 0.8475 N (table 1).

In both helmets, a higher drag was noted at 90º angle of attack, when compared to a 0º angle.

The time trial helmet presented higher aerodynamic drag compared to the track model at 90º. These are kept for all velocities selected though. However, at 0º time trial helmet presented lower drag compared with the track one.

Table 1. Drag force at different velocities and attack angles.

Velocity	**Track Helmet (Fd)**		**Time trial Helmet (Fd)**	
[m/s]	**[N]**		**[N]**	
	0º	90º	0º	90º
2.0	0.0884	0.0899	0.0660	0.1025
3.5	0.2139	0.2474	0.1615	0.2659
5.0	0.4012	0.4607	0.3116	0.5423
6.5	0.6675	0.7323	0.4667	0.8475

3.4. Discussion

The obtained aerodynamic drag ranged from 0.0660 and 0.8475 N. Some authors presented similar results, near 1 N. However, reports in the literature assessed the performed at velocities higher than 6.5 m/s and the rider shoulders were also included in the simulations (Alem et al., 2014). A higher surface area (because the shoulders were scanned) will contribute for a higher aerodynamic drag.

Others reported 0.319N of drag force for a time trial helmet. This data is in accordance to our outputs. However, it should be noted that they run the simulation only for the helmet (i.e., without scanning the head) but at a higher velocity (13.4 m/s or faster) (Sidelko, 2007).

3.5. Conclusion

Wheelchair racing athletes might wear time trial helmets when they keep looking forward. In the event of looking downwards, the aerodynamic drag will increase meaningfully in comparison to track helmet. Thus, racers should be aware of this drawback wearing time trial models.

CFD methodology might be useful for better understanding the technical features intending to optimize athlete's performance. Namely with, different helmets, speeds and angles of attack study. Futures researches could evaluate and create customized helmets for each athlete in agreement with his characteristics.

3.6. Practical Applications

The helmets use seems to be one of the strategies to reduce drag in wheelchair racing athletes. A time trial helmet, should be used by athletes for short or long distances. The athletes must look forward with a time trial helmet. A neck flexed position during the race will increase the surface area and drag. Thus, for a time trial helmet use, coaches should perform training sessions for the garments adaptation. This technic training should intend to help the athlete to maintain the head raised, with the neck in hyperextension with a helmet use.

Chapter 4. The variations on the aerodynamics of a world-ranked wheelchair sprinter in the key-moments of the stroke cycle: a numerical simulation analysis.

Abstract

Biomechanics plays an important role helping Paralympic sprinters to excel, where the aerodynamic drag has a significant impact on athlete's performance. Thus, the aim of this study was to assess the aerodynamics in the different key-moments of the stroke cycle by Computational Fluid Dynamics. A world-ranked wheelchair sprinter was scanned on the racing wheelchair wearing his competition gear and helmet. The sprinter was scanned in three different positions: (i) catch (hands in the 12h position on the hand-rim); (ii) the release (hands in the 18h position on the hand-rim) and; (iii) recovery phase (hands do not touch the hand-rim and are hyper-extended backwards). After the numerical simulations computation, mean viscous and pressure drag components and total drag force were retrieved. The simulations were performed at 2.0, 3.5, 5.0 and 6.5 m/s. The values for viscous drag ranged from 3.35 N to 2.94 N, pressure drag from 0.38 N to 5.51 N, total drag force from 0.72 N to 8.45 N and effective area from 0.24 to 0.41 m^2. The results demonstrated that less drag is obtained in the recovery phase, in opposing to higher drag at the catch. This reinforces the importance on maintaining an adequate body alignment to avoid drag increase.

Keywords: CFD, wheelchair racing, aerodynamics, drag.

4.1. Introduction

Wheelchair sprinting events are some of the most popular races in Paralympics. In these events, athletes compete on racing wheelchairs designed to let them reach their maximal speed (Forte et al., 2017).

Biomechanics plays an important role helping Paralympic sprinters to excel. The proper alignment of the body segments and a good stroke technique will help to reduce the winning time (Forte, Barbosa & Marinho, 2015). To reach the maximal acceleration as soon as possible and maintain a maximal speed over the race, the resistive forces must be minimized and propulsive forces maximized (Forte, Barbosa & Marinho, 2015; Fuss, 2009). The propulsive forces (pushing the hand-rim and the wheels producing force on the ground), should overcome the resistive forces (i.e., the rolling friction and aerodynamic drag). Each stroke cycle can be broken-down into three key-moments. The first moment is the beginning of the propulsive phase, being the hands in the 12h position on the hand-rim (known as catch phase). When the hands are in the 18h position on the hand-rim, the propulsion phase ends (known as release phase). When the hands are not in contact with the hand-rim and hyperextended backwards, this is known as the recovery phase (Forte, Barbosa & Marinho, 2015). The propulsive phases (between catch and release) account for approximately 35% of the stroke cycle´s duration and the recovery the remaining 65% (Forte, Barbosa & Marinho, 2015).

In wheelchair racing, aerodynamic drag has a significant impact on the performance at speeds higher than 5 m/s (Cooper, 1990; Candau et al., 1999; di Prampero, 1986; Martin et al., 2006; Millet & Candau, 2002). At world record pace, drag force may account for 34.89% of the overall resistive forces (Barbosa et al., 2014). However, no study was carried out comparing the aerodynamics of a sprinter in the key-moments of the stroke cycle (i.e. catch, release and recovery phases).

It was claimed that marginal shifts in the rider's position on the wheelchair might change the drag by 10% (Ryschon & Stray-Gundersen, 1991; Mc Lean, et al., 1994; Paton, 2006). Still, there is scarce evidence on this. Barbosa et al. (2016), compared by experimental testing the resistive forces in three different head and torso positions, noting variations in the aerodynamics. Thus, the drag force may change in the key-moments of the stroke cycle depending on the relative position of the upper arms, torso and head. E.g., the change in the relative position may have influence on the surface area and, hence, on the drag coefficient.

Numerical simulations by Computational Fluid Dynamics (CFD) are arguably the best technique available to run this comparison. Benchmarked with other procedures to monitor the aerodynamics, CFD has the advantage of minimizing confounding factors such as the intra-subject variability and the changes in the environmental conditions across trials. It is possible

to control with higher accuracy the temperature, pressure and speed of each simulation. Unfortunately, the control of these factors in experimental tests is more challenging. Besides that, using CFD it is possible to breakdown the total drag force into viscous and pressure drag (Forte, Barbosa & Marinho, 2015).

Pressure drag can be characterised as the fluid distortion in the rear edges and the pressure differences between the front and back boundaries of the body (in our study the wheelchair-athlete system) (Schlichting, 1979; Debraux et al., 2011). The fluid separation from the back boundaries will generate a low pressure zone, mainly caused by the object/body shape (Schlichting, 1979; Debraux et al., 2011). The pressure drag is dependent on several factors, including the body size and geometry (Debraux et al., 2011; Kennedy & Lamo, 2013; Kyle, 2013; Harun, 2012; Defraeye et al., 201; Kulfan, 2000). As such, arguably in wheelchair racing, the athlete's position will influence the pressure drag. Nevertheless, it was not found any evidence on this in the literature.

Viscous drag is produced due to the interaction between the body's surface and the fluid (Schlichting, 1979). In the case of a fluid with viscosity, such as air, the fluid is going to stick to the body's surface and being dragged. Because of the viscosity, this layer of fluid attached to the body will make the following layer to attach to itself. Same phenomenon happens to nearby layers. Viscous drag is the force needed to drag the sum of all layers of fluid. Thus, this component is strongly dependent on the speed and surfaces roughness. Although viscous drag might have arguably a smaller impact compared to pressure drag, it has important implications on the athlete's performance. The body position, garments' design and materials used, as well as, surface's roughness will have an effect on viscous drag (Schlichting, 1979; Edwards & Byrnes, 2007). There are claims that in wheelchair racing, viscous drag can be decreased by reducing the surface roughness, for instance, wearing light and tight garments. However, no study was founded assessing viscous drag in wheelchair racing.

Effective aerodynamic area (ACd) is a well-rounded parameter to assess the aerodynamics of a body. It is obtained by the multiplication of the drag coefficient by the surface area. ACd is the area that acts in the drag-production direction (opposite direction of the flow) (Schlichting, 1979; Crouch, et al., 2017). E.g., in cycling, time trial positions are recommended to decrease the ACd (Crouch et al., 2017; Bouillod et al., 2016). Thus, ACd is mainly dependent of the athlete's surface area and position. Some studies monitored the ACd of wheelchair sprinters (Barbosa et al., 2016; Hoffman et al., 2003). Barbosa et al. (2016), observed values between 0.1456m^2 and 0.1747m^2; whereas, Hoffman at el. (2003), reported an ACd of 0.37m^2. The data reported by these authors are mean values for the entire stroke cycle. There is no evidence on the changes in the ACd in different key-moments of the stroke cycle in wheelchair sprinting.

The aim of this study was to assess the aerodynamics in different key-moments of the stroke cycle by CFD. It was hypothesised that the drag varies in different phases of the stroke cycle, depending on the relative position of the segments.

4.2. Methods

4.2.1. Subject

A world-ranked wheelchair sprinter (ranked 4th in the 100m and 400m T-52 category at the time of the data collection) volunteered to take part of this study.

Approval was granted by the Ethics Committee of the University of Beira Interior. All procedures were in accordance to the Helsinki Declaration regarding human research. A written consent by the participant was obtained beforehand.

4.2.2. Scanning the model

The sprinter was scanned on the racing wheelchair wearing his competition gear and helmet. The scans were made in three different positions (Fig 1): (i) catch (i.e., the beginning of the propulsive phase, being the hands in the 12h position on the hand-rim); (ii) the release (i.e., hands in the 18h position on the hand-rim) and; (iii) recovery phase (i.e., hands do not touch the hand-rim and are hyperextended backwards). The 12h position is set when the hand catches the hand-rim (the catch phase). In this position, the hands contact the hand-rim in an angle of about 0º to 15º with the vertical axis (i.e. on the top of the wheel). The 18h position is set when the hands leave the hand-rim (release phase). The hand contact breaks off, usually near the 180º angle with the vertical axis (i.e. on the bottom of the wheel).

The scanning was made by the 3D Artec Scanner (Artec Group, Inc., Luxembourg) and saved in the Artec Studio 0.7 (Artec Group, Inc., USA). The same software was used to edit the scans (e.g., smooth and merge all the scan layers). Upon that, Geomagic studio (3D Systems, USA) was used to mesh the object and improve it by smoothing self-intersections, clean noun-manifold edges, and spikes correction being then converted in a computer aided design (CAD) model.

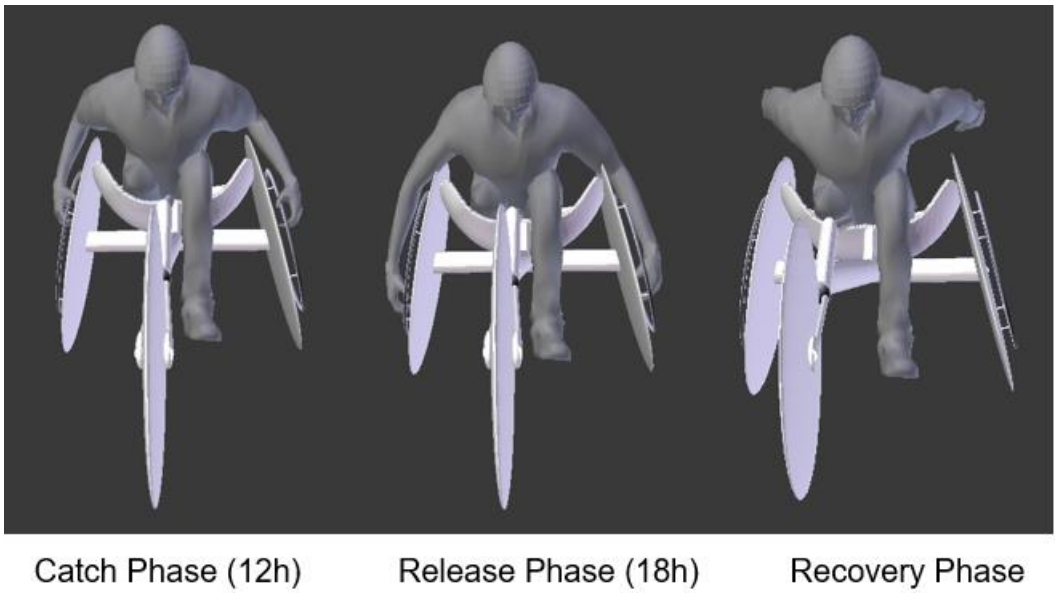

Figure 1. Three different scanned positions: (i) catch (i.e., the beginning of the propulsive phase, being the hands in the 12h position on the hand-rim); (ii) the release (i.e., hands in the 18h position on the hand-rim) and; (iii) recovery phase (i.e., hands do not touch the hand-rim and are hyperextended backwards) respectively.

4.2.3. Numerical simulation

The CAD models were imported into Fluent CFD code (Ansys Fluent 16.0, Ansys Inc., Pennsylvania, USA). The numerical simulation was underpinned by the discretization of the Navier-Stokes equations by the finite volumes methods. The Reynolds-Averaged Navier-Stokes converts instantaneous values into means. Fluent CFD code (Ansys Fluent 16.0, Ansys Inc., Pennsylvania, USA.) allowed to solve these equations using the finite volume approach, having the equations been integrated over each control volume. The behaviour of the fluid flow (equation 1), Reynolds stresses (equation 2), temperature (equation 3) and mass transfer (equation 4) have been solved as follows:

$$\frac{\partial_{Ui}}{\partial_{xi}} = 0 \tag{1}$$

$$\frac{\partial_{Ui}}{\partial_t} \pm U_j \frac{\partial_{Ui}}{\partial_{x_j}} = -\frac{1}{\rho}\frac{\partial P}{\partial x_j} + \frac{\partial}{\partial x_j}\left(2vS_{ij} - \overline{\mu_j{}'\mu_i{}'}\right) \tag{2}$$

$$\frac{\partial_{\theta i}}{\partial_t} \pm U_j \frac{\partial_\theta}{\partial_{x_j}} = \frac{1}{\rho_{cp}}\frac{\partial}{\partial x_j}\left(k\frac{\partial\theta}{\partial x_j} - \overline{\mu_j{}'\theta'}\right) \tag{3}$$

$$\frac{\partial_C}{\partial_t} \pm U_j \frac{\partial_C}{\partial_{x_j}} = \frac{\partial}{\partial x_j}\left(D\frac{\partial C}{\partial x_j} - \overline{\mu_j{}'c'}\right) \tag{4}$$

Where, μi and xi are the instantaneous velocity and the position, p is the instantaneous pressure, t is the time, ρ is the fluid density, v is the molecular kinematic viscous, cp is the heat capacity, k is the thermal conductivity, Sij is the strain-rate tensor, c is the instantaneous concentration, and D is the molecular diffusion coefficient. The Reynolds stresses component ($\overline{\mu_j'\mu_i'}$), describes the turbulence of the mean flow being the exchange of momentum by the change of the fluid parcels.

The realizable k-epsilon was the turbulence model selected for this research. This model present velocity histograms similar to standard k-ε, RST and RNG k-ε models. The latter models converged after 11876, 3208 and 2874 interactions respectively. However, earlier one (i.e. realizable k-ε) only required 1404 interactions to converge the solution, therefore, showing a higher computation economy (Aroussi et al., 2001). The aerodynamic drag force was computed as:

$$F_D = 0.5\rho A_d v^2 C_D \quad (5)$$

Where FD is the drag force, CD represents the drag coefficient, v the relative velocity, Ad surface area and ρ is the fluid density.

4.2.4. Boundary Conditions

The three-dimensional domain was meshed to depict the fluid flow around the athlete-wheelchair system (Fig 2). The whole domain (3m x 2m x 1.5m) was composed by 35 million of prisms and pyramids elements and created in the Ansys meshing module (Ansys Inc., Pennsylvania, USA).

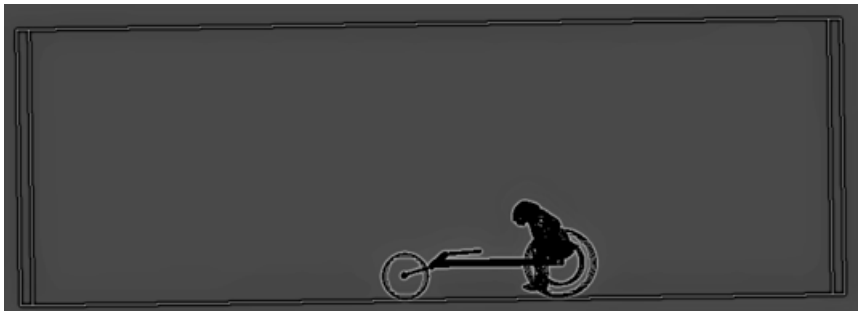

Figure 2. Wheelchair-athlete system in the enclosure.

To create an accurate model, the grid node separation in areas of high velocity and pressure was decreased (Bixler, Pease & Fairhurst, 2007; Marinho et al., 2010). The subtract operation was used to separate the wheelchair-athlete from the enclosure and define it as an object inside the tunnel. This procedure was carried out for the three different positions (catch,

release and recovery phases). The body of the athlete-wheelchair system was aligned with the z-axis direction.

The air velocity was set in the inlet portion of the dome surface (-z direction), with steady values between 2.0 and 6.5 m/s (increments of 1.5 m/s in each simulation). The turbulence intensity was set at 1×10−6%. The surface of the sprinter was modelled as a non-slip wall with zero roughness, at which scalable wall functions were assigned. The SIMPLE algorithm scheme was selected to solve the pressure-velocity coupling. For the spatial discretization, the Green-Gauss cell-based gradient was chosen (Ansys Inc, 2013). Pressure and momentum were defined as second order and second order upwind, respectively. Turbulent kinetic energy and turbulent dissipation rate were set as first order upwind.

4.2.5. Outcomes

The mean viscous and pressure drag components, total drag coefficient and total drag force were retrieved. The surface area was obtained by Geomagic studio (3D Systems, USA) and then the ACd computed.

4.3. Results

Viscous drag force ranged between 0.35 N and 2.94 N, from 2.0 m/s to 6.5 m/s, respectively (Fig 3). The highest magnitude was noted in the catch phase and the lowest in the recovery phase. The difference between catch and release phases was 3-4% across the selected speeds. The release and recovery phases differed by 1-2%. The differences between the catch and recovery phases were 3-4%. Thus, the differences between key-moments of the stroke cycle ranged between 1% and 4%.

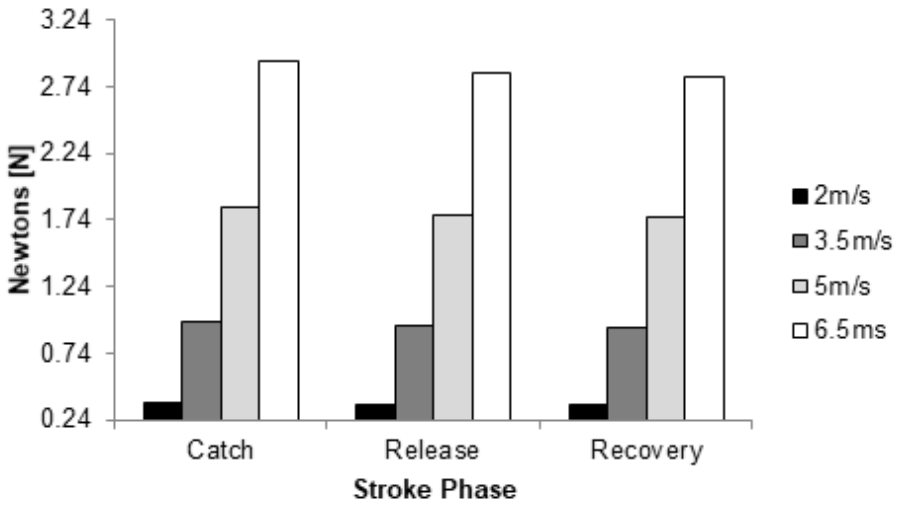

Figure 3. Viscous drag over the stroke cycle at 2.0 m/s (black column), 3.5m/s (dark grey column), 5.0 m/s (light grey column) and 6.5 m/s (white column).

The pressure drag ranged between 0.38 N and 5.51 N for the same speed range (Fig 4). The highest magnitude was noted in the catch phase; whereas, the lowest values in the recovery phase. The differences between catch and release phases were about 3% to 8% across the selected speeds. From the release to recovery phases, the differences ranged from 37% to 43%. The catch phase differed in 43% to 52% from the catch phase. Therefore, the pressure drag differed about 3% to 52% over the entire stroke cycle.

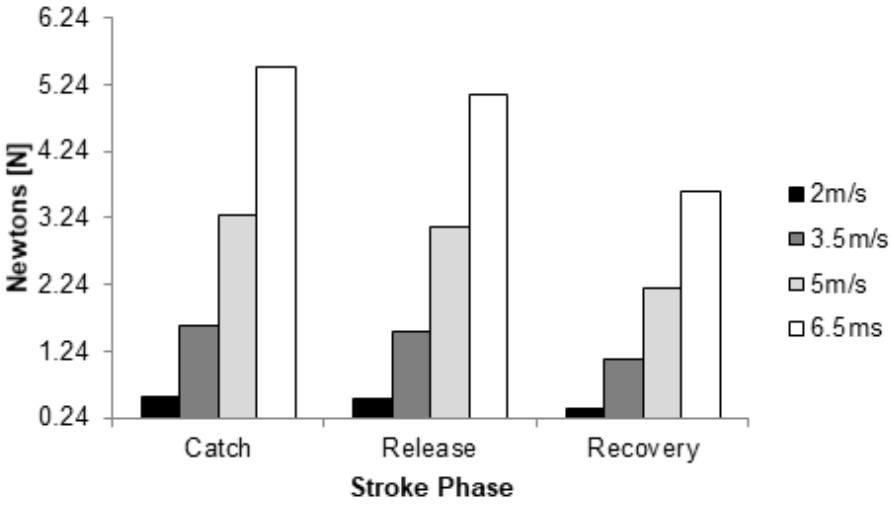

Fig 4. Pressure drag force over the stroke cycle at 2.0 m/s (black column), 3.5m/s (dark grey column), 5.0 m/s (light grey column) and 6.5 m/s (white column).

The total drag force ranged between 0.72 N and 8.45 N (Fig 5). The key-moment under less drag was the recovery, and the catch phase the highest. At the selected speeds, it was observed a decreasing drag from the catch to the release phase (3-7%). Between the release and recovery phase, total drag decreased between 21% and 24%. The catch phase differs from the recovery by 25-31%.

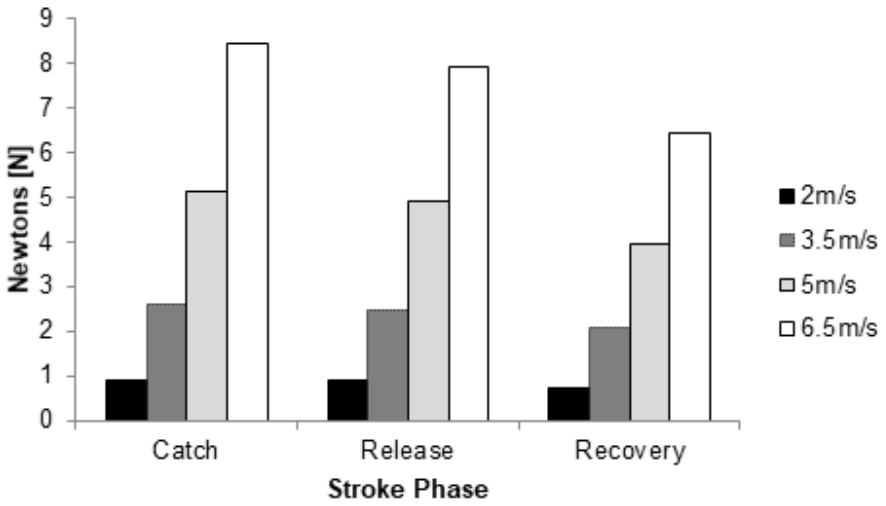

Fig 5. Total drag force over the stroke cycle at 2.0 m/s (black column), 3.5m/s (dark grey column), 5.0 m/s (light grey column) and 6.5 m/s (white column).

The ACd ranged from 0.24 to 0.41 m^2 across the selected speeds. The lowest value was noted in the recovery phase and the highest in the catch phase (fig 6). From the catch to the release phases, the ACd decreased between 7% and 17%. From the release to the recovery phase, the difference was about 21-24%. The differences between the recovery and catch phases were 30-41%. Altogether, the best ACd was of the three key-moments was found in the recovery phase.

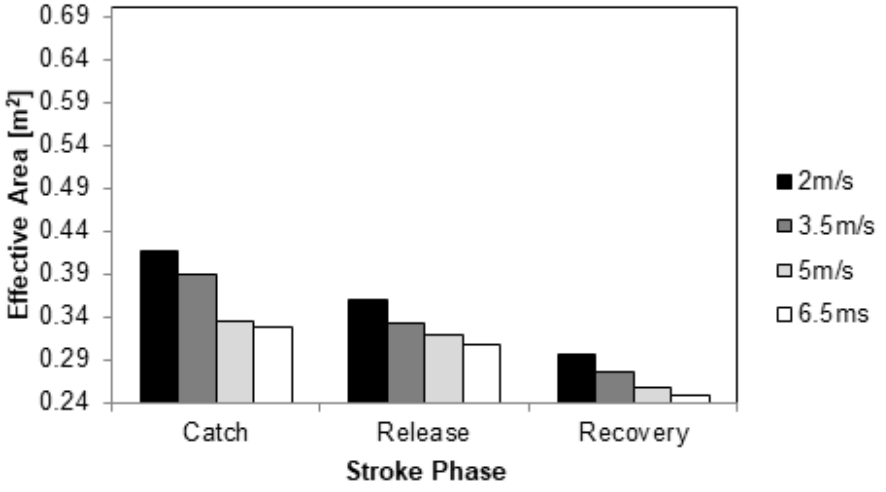

Fig 6. Effective area over the stroke cycle at 2.0 m/s (black column), 3.5m/s (dark grey column), 5.0 m/s (light grey column) and 6.5 m/s (white column).

4.4. Discussion.

The aim of this study was to compare the aerodynamics in three key-moments of the stroke cycle in wheelchair racing by CFD. The recovery phase was the most aerodynamic position, followed-up by the release and catch phases.

As above-mentioned, no research has been conducted assessing the aerodynamics of wheelchair sprinters by CFD. However, Forte et al. (2017) performed a numerical simulation of a road helmet in two different positions at speeds slower than 6.5m/s (near the typical speed reached by wheelchair sprinters in the T52 category). The ACd ranged from 0.024 to 0.034 m^2. The most aerodynamic position of the head and helmet was keeping an angle of attack of 0º (looking forward). Several studies can be found in the literature monitoring high-speed vehicles in other sports. Winkler and Pernpeintner (2010) tested the brakeman's (behind the pilot) arms position in bobsleigh. The authors reported that the bent arms position showed an ACd of 0.0596 m^2 and with the arms stretched holding the sidewalls of the bobsleigh 0.0609 m^2. The authors noted that the arms' positions influenced by about 2% the ACd. Defraeye et al. (2010) performed a numerical simulation of a cyclist in three different positions. The ACd ranged from 0.169 m^2 to 0.235 m^2. Other studies were performed evaluating the cyclists' ACd (Blocken et al., 2013; Griffith et al., 2014; Grappe et al., 1997; Defraeye et al., 2014). Blocken et al. (2013), performed an analysis of two cyclists in three different positions (upright, dropped and time-trial position) between 60 and 100km/h. The authors reported an ACd between 0.131 m^2 and 0.211 m^2. Time-trial was the most aerodynamic position. In this position the cyclists were keeping a flexed trunk and looking forward. Griffith et al. (2014), assessed the effect of the leg position on the ACd. The ACd ranged from 0.16 m^2 to 0.24 m^2 keeping symmetric and asymmetric knees alignment. The asymmetric knees alignment (one leg fully extended and the other flexed and raised close to the torso) presented the highest ACd.

The values for viscous drag ranged from 3.35 N to 2.94 N. There are no reports about viscous drag in wheelchair racing that we can use to benchmark our data. It is possible to reduce viscous drag by decreasing the surface roughness, for instance, wearing specific garment. Viscous drag in cycling is about 5% of total drag (Defraeye et al., 2010). In our study, the viscous drag ranged from 35% to 49% of total drag. The higher contribution by viscous component to total drag in wheelchair racing in comparison to cycling can be due to: (i) maximal speed in the T52 category is about 6.5 m/s (i.e., 23.40 km/h). In cycling, performers can reach a higher speed. Studies are conducted at speeds over 60 km/h (Blocken et al., 2013) and; (ii) the surface area of an athlete-wheelchair system is larger than a bicycle-athlete system. Viscous drag is strongly dependent on the surface area, where a higher area will lead to a higher magnitude of this force. In the 12h arms position, viscous drag ranged from 0.36 N to 2.93 N. In the 18h arms position, the viscous drag varied from 0.35 N to 2.83

N. In the recovery phase, viscous drag values were between 0.34N and 2.81 N. In the 12h arms position it was noted the largest ACd. On top of that, the arms flection may had increased the surface roughness. In the 18h position, the arms were fully stretched downwards and the surface roughness might have decreased. This roughness can be due to wrinkles and folded tissue in the racing suit. Over the recovery phase, the arms are overstretched backwards and the trunk flexed forward. In this position, arguably the surface might have had a lower roughness because the arms are hyperextended backwards.

Pressure drag ranged between 0.38 N and 5.51 N. The total drag ranged between 0.72 N and 8.45 N. In cycling, the pressure drag accounts for 90% of the total drag. Apparel, such as helmets, may help to reduce pressure drag (Forte et al., 2017). Authors also reported that pressure drag is the main contributor for total drag in cycling, running and swimming (Barbosa et al., 2014; Faria, Parker & Faria, 2005; Barbosa et al., 2017). In our study, pressure drag had a contribution of 51-65% to total drag. Again, this might be caused by the wheelchair-athlete surface area and the selected speeds. At higher speeds, pressure drag is prone to increase meaningfully. In this study, pressure drag varied in 12h arms position between 0.54 N and 5.51 N. In the 18h position, the differences were between 0.52 N and 5.09 N. In the recovery phase pressure drag values ranged between 0.34 N and 2.91 N. Pressure drag is generated by the pressure differences between the front and back boundaries of the body (in our case the wheelchair-athlete system) (Debraux et al., 2011; Kennedy & Lamo, 2013; Kyle, 2013; Harun, 2012; Defraeye et al., 201; Kulfan, 2000). The recovery phase had the lowest pressure drag because the sprinter kept the upper-arms hyperextended backwards. In this position, the total length of the wheelchair-athlete system (length from the front wheel to the tip of the fingers extended backwards in the horizontal plane) increases slightly. Moreover, the geometry of the system is modified, keeping a more aerodynamic position (lower angle of attack by the upper-body) and decreasing the ACd. On the other side, in the 18h position the overall geometry of the system increases the surface area. The upper-body is in an upright position and the upper-arms fully extended and facing downwards, increasing the area exposed on the direction of displacement.

The ACd values ranged from 0.24 to 0.41 m^2 across the selected speeds. Barbosa et al. (2016) noted an ACd of about 0.15 m^2 in one elite wheelchair racer. The authors tested aerodynamics by coast-down technique. Hoffman et al. (2003), tested five different wheelchairs also by the coast-down technique, noting a value of 0.37 m^2. Our findings (ACd: 0.24-0.41 m^2) are in alignment with these latter results. In our study, ACd varied in the 12h position from 0.32 m^2 to 0.41 m^2. In the 18h position, ranged between 0.31 m^2 and 0.35 m^2. In the recovery phase the ACd values were between 0.24 m^2 and 0.29 m^2. The ACd is the wheelchair-athlete system area that acts in the drag-production direction (Bouillod et al., 2016). Thus, it is possible to argue that the different positions influenced the drag force (Crouch et al., 2017; Bouillod et al., 2016). The 12h arms position presented the highest drag-

production area. In the 18h arms position, the trunk flection and the arms near the hand-rims seem to explain the decrease in the drag-production. The same might had occur in the recovery phase; despite the trunk flection and the arms in a hyperextended backwards position decreased ACd and the drag-production area. The drag coefficient (and as such the ACd of our sprinter) is affected by Reynolds number. In this study, our subject showed a Reynolds number of 2.82×10^5, 4.93×10^5, 7.04×10^5 and 9.15×10^5 at 2.0, 3.5, 5.0 and 6.5 m/s, respectively. For several bodies it is noted a significant drop in the drag coefficient at Reynolds number of 10^5 (Schlichting, 1979; 37]. E.g., in a sphere the drag coefficient decreased from about 0.6 to 0.4 increasing the Reynolds number between 4×10^5 and 8×10^5 (Schlichting, 1979). At Reynolds number between 2×10^6 and 8×10^6 the drag coefficient decreased from 0.5 to 0.1 (Munson, Young & Okiishi, 1990). This effect is known as "drag crisis" and it is associated with the separation of the boundary layer from the surface of the sphere (Munson, Young & Okiishi, 1990). Similar phenomenon can explain why the ACd of the wheelchair-sprinter system decreased with increasing speed.

Total drag ranged between 7% and 31%. However, between the catch and release phases the differences were only 3% to 7%. It is to note that the arms' positions have a meaningful impact on the surface area. The different arms' positions may increase the surface area and, therefore, the total drag. These results seem to be in accordance with literature. Reports in cycling and wheelchair racing noted that small variations in the rider's positions may influence drag in about 10% (Ryschon & Stray-Gundersen, 1991; McLean et al., 1994; Paton, 2006). In our case, the 12h arms position had a higher surface area in comparison with 18h and the recovery phase.

In short distances, coaches should advise their athletes to perform the propulsive phase of the stroke cycle as fast and powerful as possible. This strategy aims to reduce the winning time. In elite wheelchair racers, the recovery phase represents 65% to 67% of the stroke cycle (Candau et al., 1999; Ridgway, Pope & Wilkerson, 1988; Gehlsen, Davis & Bahamonde, 1990; Cooper, 1990; Sanderson & Sommer, 1985). The remaining 33% to 35% represents the propulsive phase (Candau et al., 1999; Ridgway, Pope & Wilkerson, 1988; Gehlsen, Davis & Bahamonde, 1990; Cooper, 1990; Sanderson & Sommer, 1985). During the recovery phase, athletes should maintain a good body alignment and limbs' symmetry as much as possible to prevent an increase in the drag. The arms must be kept backwards and fully stretched. In the propulsive phase, the arms must perform the propulsion in a symmetric position and athletes must avoid spending too much time in the 12h arms position. The athletes must start a new stroke cycle as faster as possible to avoid increasing the drag. Moreover, insights on the aerodynamics can also help coaches to prescribe training sessions. E.g., designing training session or drills/sets with the goal of reducing the intra-cycle speed decay (over the recovery phase) caused by a poor body alignment.

It can be addressed as main limitations of this study: (i) the simulations were performed in static positions; (ii) one single athlete was recruited; (iii) the maximal speed selected in this study was 6.5 m/s and the average pace of the world record at the moment of the data collection was 6.62 m/s; (iv) the numerical simulations were performed assuming a temperature of 15º C and no other temperatures were tested.

4.5. Conclusion.

The obtained results shown that aerodynamics varies along the three key-moments of the stroke cycle in wheelchair racing. The position with less drag acting on the athlete-chair system was the recovery phase. The positions submitting higher drag were the catch followed-up by the release phase. These findings suggest the importance of keeping an adequate body alignment to avoid an increase in the drag force and likewise an increase of the intra-cyclic variations of the speed within the stroke cycle.

4.6. Practical Applications

During a sprinting event athletes must perform their strokes as faster and powerful as possible. This will allow to reach sooner their maximal speed. A better knowledge of aerodynamics helps coaches to advise their athletes to maintain the body alignment and synchronization during propulsion. Thus, during the recovery phase, athlete's upper limbs must assume a back and stretched position. It is also convenient to maintain a body alignment and symmetry as much as possible to prevent drag increase. Whereas, during the propulsive phase, the athlete's arms must perform the propulsion in a symmetric position. Even more, the drag knowledge may help coaches to prescribe training sessions intending to surpass the resistive forces. The training prescription based in this data's can help to reduce the intra-cycle speed decay (due the recovery phase) from the drag force.

Chapter 5. Estimation of mechanical power and energy cost in elite wheelchair racing by analytical procedures and numerical simulations.

Abstract

The aim was to compare the mechanical power and energy cost of an elite wheelchair sprinter in the key-moments of the stroke cycle. The wheelchair-athlete system was 3D scanned and then Computational Fluid Dynamics was used to estimate the drag force. Mechanical power and energy cost were derived from a set of formulae. The effective area in the catch, release and recovery phases were 0.41m2, 0.33m2 and 0.24m2, respectively. Drag increased with speed and varied across the key-moments. The catch required the highest total power (range: 62.76-423.46W), followed-up by the release (61.50–407.85W) and the recovery (60.09-363.89W).

Keywords: Paralympics, drag, sprinting, kinetics, power.

5.1. Introduction

In wheelchair racing, propulsive forces play an important role in the athlete's performance. Propulsive forces are produced pushing the wheel's handrim periodically over a race (Forte et al. 2015). In a 100 m sprint, world-ranked wheelchair racers can perform about 40 full cycles pushing the handrim (Barbosa & Coelho. 2017). After each push, the athlete must reposition the hands on the handrim to perform another cycle (Forte et al. 2015; Barbosa & Coelho. 2017). So, it is possible to breakdown each stroke cycle in two main phases: (i) propulsive phase and (ii) recovery phase. The propulsive phase is split-up in catch phase (the first contact of the hand on the handrim) and release phase (the moment that hand break off contact with the handrim). During the recovery phase, athletes usually perform an elbow flection and hyperextension of the shoulder to bring back the upper-arms forward and prepare a new push (Barbosa & Coelho. 2017).

A sprinter aims to reach the resultant maximal velocity as soon as possible, and keep it over the race. The wheelchair-athlete system is considered more efficient if it can deliver less mechanical power and/or energy cost of transportation for a given velocity or pace (Forte et al. 2015; Barbosa et al. 2016; Hoffman et al. 2003). To reach the maximal velocity, energy is required to generate motion and overcome the resistive forces (Forte et al. 2015; Barbosa & Coelho. 2017), thus:

$$v = \sqrt{\frac{2.(E_{in} - E_{loss})}{m}} \quad (1)$$

Where v is the wheelchair velocity, Ein the athlete delivered energy, Eloss the lost energy by the system and m the mass. The difference between Ein and Eloss encompasses the kinetic energy of the system (Barbosa et al. 2016).

In wheelchair racing, the main forces of energy lost (resistive forces) are the rolling friction and the drag force (Barbosa et al. 2016; Fuss 2009). Coaches and sports analysts aim to reduce the resistive forces as much as possible to improve the final race time (Barbosa et al. 2016; Fuss 2009; Barbosa et al. 2014; Forte et al. 2016). Small shifts in the rider's position and the garments used can also help reducing the drag in about 10% (Barbosa et al. 2016; Forte et al. 2016; Rushby-Smith & Douglas. 2012; Martin. 1996; Forte et al. 2015). Nevertheless, the athlete's position varies over the stroke cycle. To produce propulsion, the athlete must bend the upper-body (i.e. torso and head) from a reasonably vertical to horizontal position, looking forward and arms pushing the handrim between the twelve and eighteen hours' positions (these are known as the catch and release phases, respectively) (Forte et al. 2015). After the release, the athlete performs the recovery phase. The arms are

back overstretched and will flex forward to prepare a new catch phase. Concurrently, the upper-body may do an extension reaching a slightly vertical position. The change in the upper-body and arms' position over the entire cycle is going to affect the drag force acting on the wheelchair-racer system (Forte et al. 2015; Forte et al. 2016).

At least in cycling, small variation in the bike-rider system have a meaningful effect on the aerodynamic drag (Martin. 1996). However, there is scarce evidence on this matter in wheelchair racing (Barbosa et al. 2016; Candau et al. 1999). These drag changes in the different positions of the stroke cycle may also affect the power and energy to reach the maximal speed. At 1.80 m/s, the drag accounts to almost 5% of the total resistive forces, and at 6.30 m/s nearly 30% (Barbosa et al. 2014). The rolling resistance accounts with 95% and 70% of the total resistive forces at 1.80 m/s and 6.30 m/s, respectively (Barbosa et al. 2014).

In wheelchair racing, it is possible to monitor the resistive forces by experimental testing (e.g. coast-down tests or wind tunnel), numerical simulations (e.g. computational fluid dynamics) and analytical models (a set of formulae) (MacLeish et al. 1993; Barbosa et al. 2014; Forte et al. 2015). Upon measuring the resistive forces and the inertial characteristics of the system, a set of analytical procedures can be used to estimate the mechanical work, power and energy (Wilson. 2004). Assessing the changes in the resistive forces over the stroke cycle by any of the above mentioned methods (experimental testing, numerical simulations or analytical procedures) enables the estimation of the intra-cyclic variation of the mechanical work, power and energy in the key moments of the cycle (i.e., catch, release, recovery). As far as our understanding goes, this has not been yet reported in the literature. One previous study selected the same analytical procedure, but having as inputs data collected by coast-down technique (Barbosa et al. 2016). Nevertheless, Barbosa et al. (2016) aimed to compare the aerodynamics, mechanical work, power and energy at different racing positions (upright position, racing position with neck in flexion and racing position with neck in hyperextension) at a mean velocity of 6.298m/s (Barbosa et al. 2016). As far as our understanding goes, this study is the first attempt to run such analysis based on computational fluid dynamics (CFD) and comparing the three key-moments of the stroke cycle.

Hence, the aim was to compare the mechanical power and energy cost of transportation delivered by an elite wheelchair sprinter in the key-moments of the stroke cycle. It was hypothesized that: (i) the mechanical power and energy cost will vary in the different key-moments of the stroke cycle, and; (ii) the catch is the phase that demands more power and energy cost, followed-up by the release and then the recovery phases.

5.2. Methods

5.2.1. Participant

A male wheelchair sprinter competing in the T52 category was recruited for this research. He holds the national records in the 100 m and 400 m events, was a finalist at Paralympic Games and World Championships in these same events and is an European medallist in the 100 m event. He was wearing his race suit and competition helmet. All procedures carried out in this research are in accordance to the Declaration of Helsinki. A written consent was obtained from the participant.

5.2.2. Scanning the Model

The wheelchair-athlete system (49.16 kg) was 3D scanned (Artec Group, Inc., Luxembourg) in three different positions (Figure 1) of the stroke cycle (catch: with the hands on the handrims in the 12 h position; release: with the hands on the handrims in the 18 h position; recovery phase: with the arms hyperextended backwards and overstretched).

Artec Studio 0.7 (Artec, USA) software was used to record, smooth and merge all the scans. The Geomagic studio (3D Systems, USA) software was used to edit the merged scans into a single object without surface errors and upon than export it as a CAD model (*.iges) (Figure 1). Then, the model was imported in Fluent code (Ansys Fluent 16.0, Ansys Inc., Pennsylvania, USA) to run the numerical simulations.

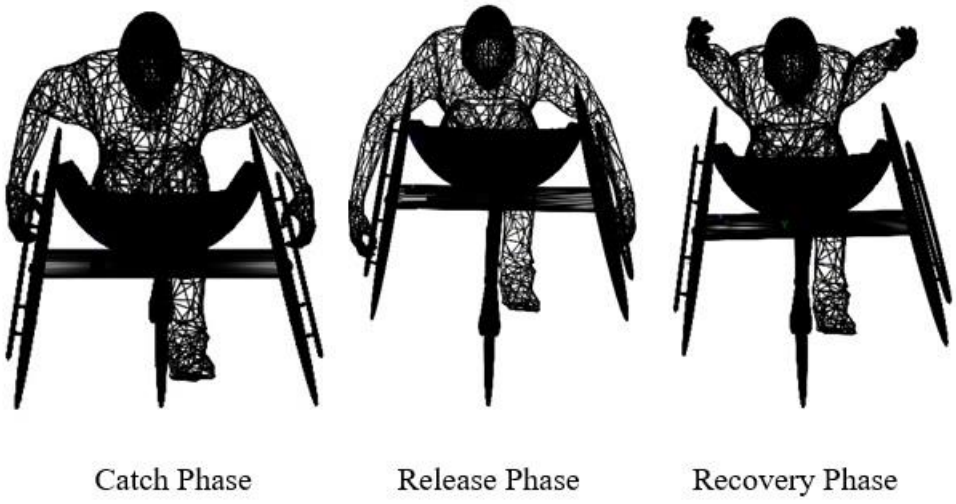

Figure 1. CAD model of the three different scanned positions: (i) catch phase; (ii) the release phase and; (iii) recovery phase respectively.

5.2.3. Boundary Conditions

The entire domain featured 35 million prismatic and pyramidal elements. The grid node separation reduction in selected areas of high velocity and pressure, allowed to generate an accurate model (Bixler et al. 2007; Marinho et al. 2010). The domain was created in Ansys meshing module (Ansys Fluent 16.0, Ansys Inc., Pennsylvania, USA) with a tunnel form (3 m length, 2 m height and 1.5 m width). The boolean subtract action was made to separate the wheelchair-athlete from the enclosure, this procedure defined that the wheelchair-athlete was an object (i.e., body) inside the tunnel. The described procedure was repeated for the three key-moments of the stroke-cycle (i.e., catch, release and recovery phase).

The air velocity was set in the –z direction and in the inlet portion of the dome surface. The initial velocity of the numerical simulations was set at 2 m/s with increments of 1.5 m/s up to 6.5 m/s. The fluent (Ansys Fluent 16.0, Ansys Inc., Pennsylvania, USA) post process allowed the estimation of the aerodynamic drag (Forte et al. 2015).

5.2.4. Numerical Simulation

The CFD simulations encompassed the discretization of the Navier-Stokes equations by the finite volumes approaches. The equations result from Newton's Second Law where in mechanics, the fluid stress is the sum of the diffusion of its viscosity. This diffusion of its viscosity results from an applied pressure term (Marinho et al. 2012; Marinho et al. 2011). The Reynolds-Averaged Navier-Stokes converts instantaneous values into means. The fluid flow behaviour (equation 2), Reynolds stresses (equation 3), temperature (equation 4) and mass transfer (equation 5) are then solved:

$$\frac{\partial_{Ui}}{\partial_{xi}} = 0 \tag{2}$$

$$\frac{\partial_{Ui}}{\partial_t} \pm U_j \frac{\partial_{Ui}}{\partial_{x_j}} = -\frac{1}{\rho}\frac{\partial P}{\partial x_j} + \frac{\partial}{\partial x_j}\left(2\nu S_{ij} - \overline{\mu_j{}'\mu_i{}'}\right) \tag{3}$$

$$\frac{\partial_{\theta i}}{\partial_t} \pm U_j \frac{\partial_\theta}{\partial_{x_j}} = \frac{1}{\rho_{cp}}\frac{\partial}{\partial x_j}\left(k\frac{\partial\theta}{\partial x_j} - \overline{\mu_j{}'\theta'}\right) \tag{4}$$

$$\frac{\partial_C}{\partial_t} \pm U_j \frac{\partial_C}{\partial_{x_j}} = \frac{\partial}{\partial x_j}\left(D\frac{\partial C}{\partial x_j} - \overline{\mu_j{}'c'}\right) \tag{5}$$

Fluent CFD code (Ansys Fluent 16.0, Ansys Inc., Pennsylvania, USA) was selected to run the above mentioned simulations. To represent the domain and fluid flow around the wheelchair-athlete system, a 3D grid or mesh with divided cells was formed in Ansys Meshing module (Ansys Fluent 16.0, Ansys Inc., Pennsylvania, USA).

The realizable k-epsilon was selected as turbulence model. This model delivered velocity histograms identical to the standard k-e model, RST and RNG k-e model. Standard k-e, RST and RNG k-e models used to converge after 11876, 3208 and 2874 interactions respectively. Moreover, as far as computation economy is concerned, the realizable k-epsilon is much more efficient because the solutions converge after 1404 interactions (Pogni & Nicola. 2016) (Pogni and Nicola, 2016).

5.2.5. Drag force

Total aerodynamic drag (Fd) and frontal surface area were retrieved from Fluent code (Ansys Fluent 16.0, Ansys Inc., Pennsylvania, USA) software.

To compute the drag force, equation 6 was used:

$$F_D = 0.5\rho A_d v^2 C_D \quad (6)$$

where, Fd is the drag force, CD represents the drag coefficient, v the velocity, A the surface area and ρ is the air density. The effective area (ACd) was calculated by the multiplying CD by A. The A was extracted also from Fluent software.

5.2.6. Mechanical Power and Energy Cost

The power to overcome drag was calculated at the selected speeds as (Barbosa et al., 2016):

$$Pd = Fd.v_x \quad (7)$$

Where Pd is the power to overcome drag, Fd the drag force and vx the horizontal velocity.

The assumed gross efficiency of wheelchair racers was 18% (Barbosa et al., 2016; Candau et al., 1999). The assumed CR was 0.01 as reported for this same participant in another paper (Barbosa et al., 2016; Barbosa and Coelho, 2017). The power output (i.e. energy expenditure per unit of time), the energy cost (i.e., energy expenditure per unit of distance) and the external mechanical power delivered were estimated as (Cooper et al., 2003):

$$Ptot = \frac{CR.m.g.v + \frac{\rho}{2}.A.C_D.v^3}{n} \quad (8)$$

$$C = \frac{CR.m.g + \frac{\rho}{2}.A.C_D.v^2}{n} \quad (9)$$

$$Pext = CR.m.g.v + \frac{\rho}{2}.A.C_D.v^3 \quad (10)$$

Where, Ptot is the total power, CR the rolling coefficient, m the body mass of the wheelchair-sprinter system, g the gravitational acceleration, v the mean velocity over the race, ρ the air density, A is the surface area and CD the drag coefficient, C the energy cost, Pext the external mechanical power and η the gross efficiency.

5.3. Results

Figure 2 reports the Pd, Ptot, C and Pext per unit of distance in the key-moments of the stroke cycle at the selected speeds. The Fd increased with speed, ranging between 0.72 N and 8.45 N. The recovery phase showed the lower drag intensity, followed by the release and then the catch phases. The Fd decreased from the catch to the release phase between 3% and 7% and, from the release to the recovery in about 21% to 24%. The increase from the recovery to catch phase was 25-31%. The ACD values were 0.24m^2 in the recovery phase, 0.33m2 in the release phase and 0.41m^2 in the catch phase.

The power to overcome drag also increased with speed and ranged between 1.45 W and 54.93 W. The recovery phase presented the lower power to overcome the drag, followed by the release phase. The catch phase presented the highest values. Between the catch and release phase, Pd decreased about 3% to 7%. Between catch and recovery phase decreased by 25% to 31% and from the release to the recovery phases between 21% and 24%.

The total power varied from 60.09 W to 423.46 W and increased with speed. The lowest values were observed in the recovery; whereas, the highest Ptot were noted in the catch phase. The differences between the catch and release were about 3% to 7% across selected speeds. The catch phase differed from the recovery phase about 8% to 21%. The differences between the release and recovery phases were about 4% to 15%.

The external mechanical power values ranged from 10.82 W to 76.22 W across the different positions and increased with speed. The phase showing less Pext being delivered was the recovery. The catch phase presented the highest Pext. The catch phase differed from the

release phase in about 3% to 8% and from the recovery phase in approximately 7% to 21%. Between the release and recovery phase differences were about 4-15%.

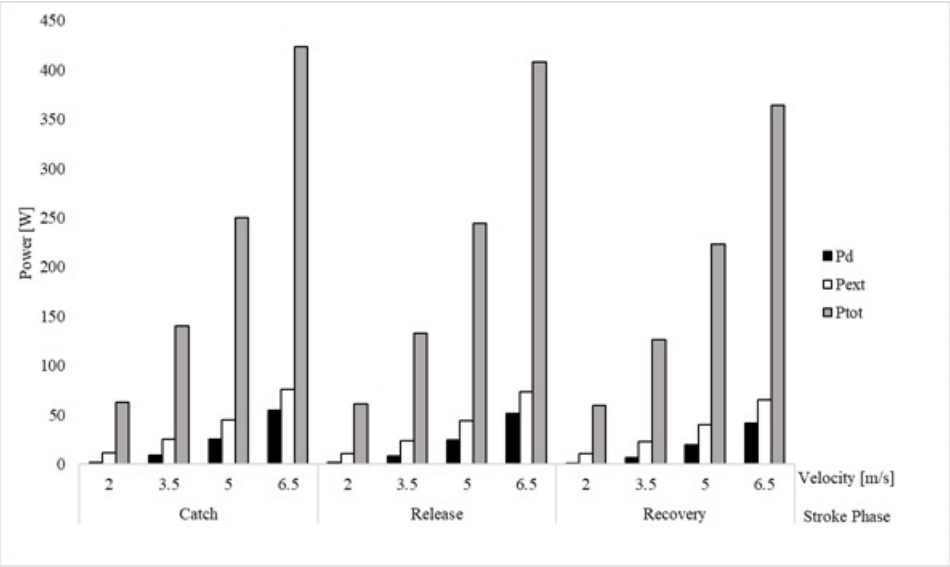

Figure 2. Power to overcome drag (Pd), external mechanical power (Pext) and total power (Ptot) in the three key-moments of over the stroke cycle at 2.0, 3.5, 5.0 and 6.5

The C ranged between 33.33 J/m and 276.26 J/m. The key-moment that demanded less C, at the selected speeds, was the recovery phase; conversely, the catch phase demanded the highest cost. From the catch to the release, differences were about 6% to 12%. From the catch to the recovery phase, C decreased between 13% to 30%. The release phase differed from recovery phase about 6% to 21%.

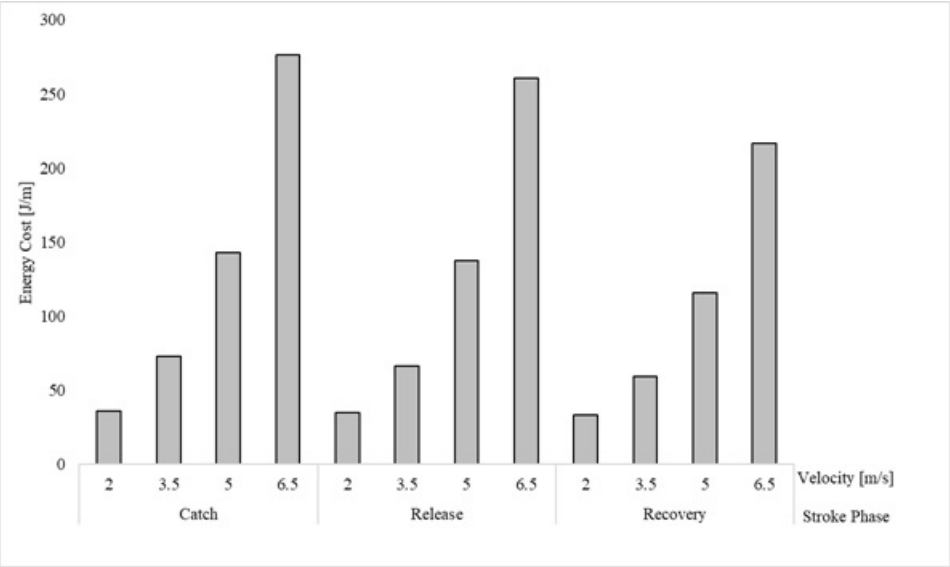

Figure 3. Energy cost (C) over the three key-moments of the stroke cycle at 2.0, 3.5, 5.0 and 6.5 m/s.

5.4. Discussion

The aim of this study was to compare the mechanical power and energy cost of transportation delivered by an elite wheelchair sprinter in key-moments of the stroke cycle. The main findings were that: (i) the mechanical power and energy cost of transportation varied in the different key-moments of the stroke cycle; (ii) the catch was the phase that required more power and energy cost followed-up by the release and then the recovery phases.

A wheelchair for team sports was noted as having a CR between 0.015 on a carpet, and 0.005 on wood floor (Chua et al. 2010). A standard wheelchair had a different CR on hard surface, smooth surface and carpet, depending of the wheel's type (0.001 in soft caster on hard and smooth surfaces and 0.007 of solid tire on a carpet) (Sauret et al. 2012). Similar CR was reported for five different types of wheelchairs on linoleum and carpet (0.0013 on linoleum for a racing wheelchair and 0.0212 of a folding wheelchair on linoleum) (McLean et al. 1994). Our assumption was a CR of 0.01 as measured by experimental testing on this same participant early on (Barbosa & Coelho. 2017; Barbosa et al. 2016; Hoffman et al. 2003). Other assumptions were a temperature of 15ºC and density of 1.225 kg/m^3. This same temperature and density were also noted by Blocken et al. (2016) for road cycling. Indeed, this environmental conditions are Fluent's default values (Ansys Fluent 16.0, Ansys Inc., Pennsylvania, USA) (ANSYS, 2013).Gross efficiency was assumed to be 18% as noted in the literature (Cooper et al. 2003; Vanlandewijck & Thompson. 2011). E.g., Cooper et al. (2003) tested twelve elite wheelchair racers on a computer monitored wheelchair dynamometer. The authors reported a gross mechanical efficiency of 18% as well. Vanlandewijck & Thompson (2011), also reported a gross mechanical efficiency of wheelchair racers between 15% and 23%.

The drag ranged between 0.72 N and 8.45 N. These results seem to match the range reported using cost-down techniques (Barbosa et al. 2016; Hoffman et al. 2003). Hoffman et al. (2003) noted an ACD of 0.37 m^2. Barbosa et al. (2016) studied the ACD of a racing wheelchair in three different racing positions by cost-down and photogrammetric techniques. The ACD ranged between 0.1456 m^2 and 0.1747 m^2. In cycling and wheelchair racing it is noted that small variations in the rider's positions may influence drag in about 10% (Rushby-Smith & Douglas. 2012; Martin. 1996; McLean et al. 1994). The ACD ranged between 0.24 m^2 and 0.41 m^2. These values seem to be in accord with findings by Hoffman et al. (2003). Even so, in our research, at 6.5 m/s, the differences between the ACD and the values reported by Barbosa et al. (2016), at a racing position was almost 0.2 m^2. The difference can be explained by the testing techniques selected (numerical simulations vs cost-down), testing conditions (comparison of the key-moments in the stroke cycle vs comparison of different racing positions) and inputs or assumptions (e.g. different climacteric conditions selected as inputs). The ACD values in our study are dependent of athlete's anthropometry and individual

characteristics. The catch phase showed the highest Fd. It differed from the release between 3% and 7% and from the recovery between 25 and 31%. The release phase had higher values than recovery in about 21% to 24%. These differences can be explained by the surface area in the different phases of the stroke cycle. The catch phase had a larger surface area when compared to the release; whereas, the release phase had a larger surface in comparison to the recovery phase. The increase in surface area in the catch phase might be due the arms position (elbow flection and with lateral projection). In the release phase, the subject upper-limbs were stretched and closed to the handrims. In the recovery phase, the upper limbs were overstretched backwards.

The power to overcome the resistive forces had been studied in wheeled vehicles (Barbosa et al. 2016; Hoffman et al. 2003; Candau et al. 1999). In cycling, the Pd ranged between 10 W at 1.2 m/s and 80 W at 5.5 m/s (Candau et al. 1999). In wheelchair racing, Barbosa et al. (2016) reported that less power was needed to overcome the drag in the racing positions with the neck in hyperextension (22.19 W). In this study, in a similar position and at 6.5m/s the power to overcome the drag was 54.93 W. Firstly, the relationship between power and speed is cubed (Pd=D.v=k.v2.v=k.v3). Secondly, the ACD reported by these authors was smaller than the one obtained in this study. The chair and garment used by the athlete was different in both studies. Others aimed to assess the resistive forces by coast-down in different types of wheelchairs (Hoffman et al. 2003). In a racing wheelchair at 5m/s, Pd was 35 W. However, after the acceleration the subject placed the hands on his knees and the torso was kept in the upright position (Hoffman et al. 2003). This position increases the surface area and hence, the Pd. Despite the difference, and considering that the subject was not in a racing position, the results seem to match ours. At 5m/s, the Pd was 25.59 W, 24.45 W and 19.67 W in the catch, release and recovery phases, respectively. Between positions, the catch phase had the highest Pd, followed by the release and then the recovery phase. Pd is dependent on the speed and Fd (equation 6). Thus, a poor aerodynamic position will require an increase in the Pd.

Barbosa et al. (2016) reported a total power between 602.55 W and 630.71 W at 6.238 m/s in different racing positions. Pelland-Leblanc et al. (2013) noted the power transfer evaluated by an optical encoder on a track, reporting a mean value of 555 W at 5.34 m/s. These results seem to match what was obtained at 6.5 m/s. Breaking down by key-moments of the stroke phase, the catch phase demanded the highest Ptot and the recovery the lowest. The catch phase presented a higher drag due the arms position near the handrims. The elbows flexion and abduction in the catch phase increased the wheelchair-athlete's width. A higher width may lead to a higher surface area and a higher Ptot is required to surpass drag. In our study, Ptot increased with speed.

The energy cost reported by Barbosa et al. (2016) ranged between 95.67 J/m and 100.14 J/m. Abel at al. (2003) assessed the energy cost on handbiking and wheelchair racing by

spirometry in an endurance test. At almost 6 m/s, the C was on average 95.55 ± 19.14 J/m. These results seem to be in tandem to our data. Therefore, our estimation seems to be a good approximation. At 5 m/s the C ranged between 142.98 J/m and 115.99 J/m, depending on the position adopted. The catch phase imposed the highest energy cost in comparison to release and recovery phases. The recovery phase led to the lowest energy cost. Because there is no propulsion been applied on the handrim, one may argue that the C should be almost null, or at least, neglectable. Nevertheless, the wheelchair-athletes keeps its motion due the inertia. Thus, the system's motion will not stop unless the resistive forces overcomes the inertial force. At each propulsive phase, the inertial force increase and allows to keep the wheels in motion during the recovery phase. In our study, the C increased with speed. Also in handbiking, the C increased with speed (Abel et al., 2003). In cycling, it was possible to observe that different positions lead to a higher or lower energy cost (Ryschon & Stray-Gundersen, 1991). The standing position presented a higher energy cost compared to a sitting position when monitored by the measurement of the oxygen uptake. The standing position presented a larger surface area and a higher energy cost. In our study the position with the largest effective area also denoted the highest energy cost.

The external mechanical power ranged between 10.82 W and 76.22 W. Barbosa et al. (2016), noted a variation between 108.51 W and 113.59 W for different racing positions. It is to point out that the authors presented a higher Pext in comparison to our results. In a study on basketball wheelchairs, the Pext was evaluated on a roller ergometer in two different time periods (Theisen et al. 1996). The mean Pext was calculated during 15 cycles in each stage and was computed by the momentary torque and angular velocity in the rear wheels. The exercise test was continuous with stages of three minutes. The subjects started at the tests at 0.58 m/s with increments of 0.28 m/s. The subjects did not reach their maximal capacity in the same stage, four reached 1.94 m/s, six reached 2.22 m/s and one was able to continue up to 2.50 m/s. Pext values ranged between 12 W and 63 W over the incremental protocol.The mean Pext values were 50.92± 6.02 W and 50.73± 5.74 W. In our study, Pext ranged between 10.82 W and 11.30 W at 2 m/s. might be explained by the fact that racing wheelchairs require less power to reach a higher speed. The maximal speed reached in basketball wheelchair was 2.5 m/s and in racing wheelchair almost 7 m/s.

Altogether, the ACD and speed play important roles in Fd, Pd, Ptot, C and Pext (equations 6, 7, 8, 9 and 10). The evaluated variables increased with speed. This was expected hence Fd, Pd, Ptot, C and Pext are speed dependents. The variables also varied in the different key-moments of the stroke cycle. That was explained by the effective area differences between positions. Positions with higher surface area and effective area lead to higher drag and required a higher Pd, Ptot, C and Pext to surpass the resistive forces.

Athletes' technique and muscle strength are determinant to deliver maximal power. So, they must be advised to enhance muscular strength and power, to perform explosive pushes in

each stroke cycle (Barbosa and Coelho, 2017). In the 100m event in the T52 category, it is hard to reach the maximal muscular power and speed due to the athletes' handicap. Thus, they must start the race performing, faster and explosive pushes (Barbosa and Coelho, 2017). For instance, these results may help coaches and athletes to design training sets at the required muscle power for a given speed or pace (i.e., sets of 15 seconds at 423 W).

The main limitations of this study were: (i) a set of assumptions were used to run the calculations (the rolling resistance, temperature, density and gross efficiency); (ii) the participant recruited is only representative of world-class athletes and not counterparts of other tiers; (iii) a comparison of mechanical power and energy cost estimation by numerical simulations and experimental testing (e.g., wind tunnel) is suggested.

5.5. Conclusion

The resistance acting upon the wheelchair racing sprinter increased with speed and varied across the different key-moments of the stroke cycle. The mechanical power and energy cost increased with speed. The phase demanding more power and energy cost was the catch phase, followed-up by the release and then the recovery phases. Athletes should maintain a proper body alignment and synchronization during the stroke cycles, enabling to reach and keep a maximal speed with a lower energy cost. Coaches and other practitioners can use these findings to carry out and evidence-based practice helping the athletes to improve their efficiency.

5.6. Practical Applications

Coaches should be aware that the stroke technique and muscle strength are determinant factor to improve speed. Training these two variable it becomes easier for athletes to accelerate and overcome inertia. Increasing the muscle power will allow produce explosive movements, determinant at the beginning of the race.

Chapter 6. General Discussion

The aim of this thesis was to assess the aerodynamics of a world-ranked wheelchair racer by computer fluid dynamics. In addiction it was intended to verify the helmets impact on drag. Our findings were that time-trial helmets had lower drag than track helmets. However, athletes must look forward using a time trial helmet; whereas, if they perform a neck flection during the race, a track helmet is recommended. Analysing the different positions that the athletes adopt during a race (key-moments during a stroke cycle), the recovery phase presented the lower drag, followed by the release phase and then, the catch phase. Our data showed that the aerodynamics of a world-ranked wheelchair racer vary in the different key-moments of the stroke cycle. Even more, athletes must wear a time-trial helmet and looking forward during the sprinting events. The body alignment and synchronization during the strokes must be a concern for athletes and coaches intending to reduce drag.

The first step of this thesis was to conduct a review that comprised the published studies on aerodynamics in wheelchair racing. Chapter 2 allowed noting that the knowledge about the wheelchair-racing aerodynamics was scarce. It was possible to find information about: (i) the main determinants in wheelchair racing; (ii) the effect of aerodynamic force in wheelchair racing performance; (iii) tools like analytical models, experimental testing, and numerical simulations to evaluate the resistive forces in wheelchair racing; and (iv) report the existence and appliance of the numerical simulations on equipment and techniques. However, no study was founded testing wheelchair racing aerodynamics by computer fluid dynamics. The main determinants in wheelchair racing are the propulsive and resistive forces. The propulsive force is the push on the handrim, producing motion (i.e. the applied force by the ground in the wheel). The resistive forces are the Fr and Fd (Fuss, 2009). The propulsive stroke cycle can be split up in propulsion phase (catch of the hands on the handrims, drive and release) and recovery phase (Fuss, 2009). Thus, it is possible to identify three key-moments in the stroke cycle, the catch and release phases and the recovery phase. Some analytical models can be founded in literature assessing aerodynamics in wheelchair racing (Forte et al., 2015). Wind tunnel tests have also been performed in wheelchair racing (MacLeish, Cooper, Harralson & Ster, 1993). Even more, coasting deceleration methods had also been used in this sport (Barbosa et al., 2014; Barbosa et al., 2016).

CFD methodology has already been used for equipment tests in wheeler riders' helmets. CFD can provide information about the helmets (Pinnoji & Mahajan, 2006). Some tests revealed that the most drag came from the athlete and that small shifts in ridder position could save 10% of the aerodynamic drag (Rushby-Smith & Douglas, 2012). CFD can be applied in different fabrics, helmets and wheelchairs. Also different rider's positions must be analysed, like the head position during the race (flexed head in the start of the race or the look forward

position). The fluid flow analysis in each stroke phase should also be analysed aiming to reach the ideal motion in the stroke phase and recovery one (Barbosa et al., 2014). Thus, CFD analysis should be performed to fulfil the lack of literature in this area.

The literature presents some studies testing helmets by CFD. However, the studies were performed at higher speeds than in wheelchair racing. Thus, aiming to test equipment's wear by wheelchair racing athletes, numerical simulations on a track and time trial helmet was performed until 6.5 m/s. This aimed to compare two different helmets (track vs time trial) at different speeds and head positions by CFD.

In the Chapter 3 the aim was to compare two different helmets (track vs time trial) at different speeds and head positions by CFD. The drag ranged from 0.0660 to 0.8475 N. Arlem et al. (2014), reported drag value near 1 N. However, the selected velocities were higher than 6.5 m/s and the rider shoulders were also included in the simulations. Others were in accordance with our results, reporting 0.319 N of drag force for a time trial helmet. However, the simulation was performed only for the helmet (i.e., without scanning the head) but at a higher velocity (13.4 m/s or faster) (Sidelko, 2017). Time trial helmets produced less drag in the looking forward position. Thus, wheelchair racing athletes might wear time trial helmets if they keep looking forward during the race.

Chapter 3 provided details on the best helmet to be selected racing a sprinting event. However, the athlete's position on the wheelchair during the race remains to be analysed. That said, a new study was designed to assess the aerodynamics of a wheelchair-athlete system.

The aim of chapter 4 was to compare the aerodynamic intra-cyclic variation in three key-moments of the stroke cycle in wheelchair racing by CFD. The recovery phase was the most aerodynamic position, followed by the release and catch phases. No research was founded assessing racing wheelchair aerodynamics by CFD. Several studies can be found in the literature on other sports involving high-speed vehicles (Winkler and Pernpeintner, 2010; Blocken et al., 2013; Griffith et al., 2014; Grappe et al., 1997; Defraeye et al., 2014).

The values for viscous drag ranged from 3.35 N to 2.94 N. There are no reports about viscous drag in wheelchair racing. In cycling viscous drag represents roughly about 5% of total drag, and the remaining 95% is due to the pressure drag (Defraeye et al., 2010). In our study, the viscous drag ranged from 35% to 49%. The total drag ranged between 0.72 N and 8.45 N. In our study, pressure drag had a contribution of 51% to 65% to total drag. The ACd values ranged from 0.24 to 0.41 m^2 across the selected speeds. Barbosa et al. (2016), noted an effective area of about 0.15 m^2 in one elite wheelchair racer and Hoffman et al. (2003) reported an ACd for wheelchair racing of 0.37 m^2. During the recovery phase, athletes should maintain a body alignment and symmetry as much as possible to prevent drag increase. The

arms must assume a back and stretched position. In the propulsive phase, athlete's arms must perform the propulsion in a symmetric position.

Chapter 4 allowed assessing the drag of a wheelchair racing sprinter. Then, knowing the resistive forces, estimations about mechanical power and energy expenditure over an official race are possible to obtain. The aim of chapter 5 was to assess the mechanical power and energy cost in different athlete's positions.

In Chapter 5, the aim was to compare the mechanical power and energy cost of transportation delivered by an elite wheelchair sprinter in key-moments of the stroke cycle. The main findings were that: (i) the mechanical power and energy cost of transportation varied in the different key-moments of the stroke cycle; (ii) the catch was the phase that required more power.

The obtained drag ranged between 0.72 N and 8.45 N. No results were founded in the literature on the Fd of wheelchair sprinters. However, our results seem to be similar to what was reported assessing the aerodynamics by a cost-down technique (Barbosa et al., 2016; Hoffman et al., 2003). The authors noted an ACd of a racing wheelchair between 0.1456m^2 and 0.1747m^2 and 0.37m^2 respectively. In our study, ACd ranged between 0.24m^2 and 0.41m^2.

The power to overcome the resistive forces had been studied in wheeled vehicles (Barbosa et al., 2016; Hoffman et al., 2003; Candau et al., 1999). In wheelchair racing, Barbosa et al., (2016) reported that the necessary power to overcome the drag racing positions with the neck in hyperextension was 22.19 W. In this study, the power to overcome the drag was 54.93 W. It can be founded some reports in literature that report a Ptot between 555 W and 6630.71 (Barbosa et al., 2016; Pelland-Leblanc et al., 2013). In our study Ptot ranged between 60.09 W and 423.46 W. In literature, the energy cost by wheelchair racing and handbiking athletes varied between 95.55 and 100.14 J/m (Barbosa et al., 2016; Abel at al., 2003). Our estimation seems to be a good approximation. At 5 m/s the C ranged between 142.98 J/m and 115.99 J/m. The external mechanical power ranged between 10.82 W and 76.22 W. Barbosa et al., (2016), noted a variation between 108.51 W and 113.59 W for different racing positions. It is to note that the authors presented a higher Pext compared to our simulations. The resistance acting upon the wheelchair racing sprinter increased with speed and varies across the different key moments of the stroke cycle. The mechanical power and energy cost increased with speed. The phase demanding more power and energy cost is the catch phase, followed-up by the release and then the recovery phases.

Altogether, a time trial helmet imposed lower drag keeping a neck hyperextension. The athletes must keep looking forward wearing a time trial helmet. The Athletes must be aware that the aerodynamics varied over the different phases of the stroke cycle. Finally, the mechanical power and energy cost in elite wheelchair racing varied in different phases of the

stroke cycle. Power targets can be defined during a race or a set of trainings. Finally, athletes must maintain the body alignment during the stroke cycle intending to reduce drag, mechanical power and energy expenditure during a race.

Chapter 7. Overall Conclusion

7.1. Conclusions

The main findings of this thesis were:

i. There is a lack of research on wheelchair racing aerodynamics' assess by CFD (chapter 2);
ii. A time trial helmet imposed lower drag keeping a neck hyperextension (chapter 3);
iii. The aerodynamics of a wheelchair racing athlete varied over the different phases of the stroke cycle (chapter 4);
iv. The mechanical power and energy cost in elite wheelchair racing varied in different phases of the stroke cycle (chapter 5).

The main conclusion of this thesis was that it is possible to improve the aerodynamics of a wheelchair sprinter by wearing the appropriate helmet and keeping the body alignment during the stroke cycle.

7.2. Limitations

The main limitations of this thesis were:

- The recruited athlete is only representative of his category;
- The standard K-ε turbulence model was not selected for these simulations;
- The enclosures for helmet and wheelchair-athlete did not have the same formats and sizes.

7.3 Suggestions for Future Research

Suggestions for follow-up studies or spin-offs of this thesis are:

- To evaluate and design customized helmets for each wheelchair sprinter.
- To perform the numerical simulations in different categories and athletes.
- To perform numerical simulations with other wheelchair-athlete's geometries, evaluating the side-by-side drag effect during a race.

Chapter 8. References

Chapter 1. General Introduction

Duarte, E., & Santos, T. P. (2003). Adaptação e inclusão. In: Duarte, E.; Lima, S.M.T. Atividade física para pessoas com necessidades especiais: experiências e intervenções pedagógicas. Rio de Janeiro: Guanabara Koogan. p. 93-9.

Paciorek, M. J. (2004). Esportes adaptados. In: Winnick JP. Educação física e esportes adaptados. Barueri: Manole. p. 37-52.

Winnick, J. P. (2004). Introdução à educação física e esportes adaptados. In: Winnick, J.P. Educação física e esportes adaptados. Barueri: Manole. p. 3-19.

Fuss, F., Subic, A., Strangwood, M., & Mehta, R. (2014). Routledge handbook of sports technology and Engineering. Routledge. NY. USA.

UCI (2012) Cycling Regulations, Part 1 General organization of cycling as a sport. Aigle: Union Cyclist Internationale. p. 63, para . 1.3.019. Available online at: http://www.uci.ch/templates/UCI/UCI2/layout.asp?MenuId=MTkzNg&LangeId=1 (acessed 12 December 2012).

IWAS. (2008). IWAS Athletics, worldwide ranking. http://athletics.iwasf.com/. Accessed 14 Aug 2009.

IPC International Paralympic Committee (2007). IPC athletics classification manual or physical impairments 2008–2010. http://www.paralympic.org/release/Summer_Sports/Athletics/News/2007_12_07 _ClassificationManual.pdf. Accessed 14 Aug2009.

Petrushov, V. A. (1998). Improvement in vehicle aerodynamic drag and rolling resistance determination from coast-down tests. Proc Inst Mech Eng D J Automobile Eng 212:369–380

Fuss, F. K. (2009). Influence of mass on the speed of wheelchair racing. Sports Engineering, 12 (1), 41-53.

Harder, P., Cusack, D., Matson, C., & Lavery, M. (2010). Airfoild development for the trek speed concept triathlon bicycle. Trek Bicycle Corporation. Available online at http://slowtwitch.com/Downloads/TK10_SC_white_paper_lores.pdf (acessed 12 December 2012).

Marinho, D. A., Barbosa, T. M., Mantha, V., Rouboa, A. I., & Silva, A. J. (2012). Modelling propelling force in swimming using numerical simulations. In: Juarez LH (Ed). Fluid Dynamics, Computational Modeling and Applications. Pp. 439448. InTech. Rijeka.

Lyttle, A., & Keys, M. (2006). The application of computational fluid dynamics for technique prescription in underwater kicking. Portuguese Journal of Sport Sciences, 6, Suppl. 2, 233-235.

Dabnichki, P., & Avital, E. (2006). Influence of the position of crew members on aerodynamics performance of two-man bobsleigh. Journal of Biomechanics, 39, 2733-2742.

Lakomy, H. K. A., Cambell, I. & Williams, C. (1987). Treadmill performance and selected physiological characteristics of wheelchair athletes. Br J Sports Med, 21(3), 130-133.

Cooper, R. A. (1990). Wheelchair racing sports science: a review J. Rehab. Res. Develop. 27 295-312.

O'Connor, T. J., Robertson, R. N. and Cooper, R. A. (1998). Three-dimensional kinematic analysis and physiologic assessment of racing wheelchair propulsion Adapt. Physical Activ. Quart. 15, 1–14

Mos, A. D., Fowler, N. E. and Goosey-Tolfrey, V. L. (2005). The intra-push velocity profile of the overground racing wheelchair sprint start J. Biomech. 38, 15–22

Barbosa, T. M., Coelho, E. (2017). Monitoring the biomechanics of a wheelchair sprinter racing the 100 m final at the 2016 Paralympic Games. European Journal of Physics. 38.4: 044001.

Liu, H. (2002). Computational biological fluid dynamics: digitizing and visualizing animal swimming and flying. Integrative and Comparative Biology, 42, 1050-1059.

Chapter 2. Technologic Appliance and Performance Concerns in Wheelchair Racing - Helping Paralympic Athletes to Excel.

IWAS (2008). IWAS Athletics, worldwide ranking. http://athletics.iwasf.com/. Accessed 14 Aug 2009

IPC International Paralympic Committee (2007). IPC athletics classification manual for physical impairments 2008–2010. http://www.paralympic.org/release/Summer_Sports/Athletics/News/2007_12_07_ClassificationManual.pdf. Accessed 14 Aug 2009.

Depauw, K. P. (1986). Research on sport for athletes with disabilities. Adap Phys Activ Q, 3(4): 292-299.

Depauw, K. P. (1988). Sports for individuals with disabilities: Research opportunities . Adap Phys Activ Q, 5: 80-89.

Cooper, R. A. (1990c). Wheelchair racing sports science: a review. Journal of rehabilitation research and development, 27(3), 295-312.

Lakomy, H. K. A., Cambell, I. & Williams, C. (1987). Treadmill performance and selected physiological characteristics of wheelchair athletes. Br J Sports Med, 21(3), 130-133.

Ridgway, M., Pope, C., Wilkerson, J. (1988). A kinematic analysis of 800-meter wheelchair racing techniques. Adapt Phys Act Q 5(2), 96-107.

Bymes, D.P. (1983). APlm and EMG drive phase analysis of the competitive wheelchair stroke. Unpublished master's thesis, University of Alberta.

Cooper, R. A. (1990b) An exploratory study of racing wheelchair propulsion dynamics. Adapt Phys Act Q, 7(1), 74-85.

Sanderson, D. J., Sommer, H. J. (1985). Kinematic features of wheelchair propulsion. J Biomech 18(6), 423-429.

Cooper, R. A. (1990). A systems approach to the modeling of racing wheelchair propulsion. J Rehabil Res Dev, 27(2), 151-62.

Davis, R., Ferrara, M., & Byrnes, D. (1988). The competitive wheelchair stroke. NSCA Journal, 10(3), 4-10.

Higgs, C. (1985). Propulsion of racing wheelchairs. In C. Sherrill (Ed.), Sport and disabled athletes, 165-172. Champaign, IL: Human Kinetics

Chow, J. W., Chae, W. (2007). Kinematic analysis of the 100 m wheelchair race. J Biomech, 40, 2564–2568.

Costa, G. B., Rubio, M. P., Belloch, S. L., & Soriano, P. P. (2009). Case study: effect of handrim diameter on performance in a paralympic wheelchair athlete. Adapted physical activity quarterly, 26(4), 352-363.

O'Connor, T., Robertson, R. N., Cooper, R. A. (1998). Three-dimensional kinematic analysis and physiologic assessment of racing wheelchair propulsion. Adapt Phys Activ Q, 15, 1–14.

Keogh, J. W. L. (2011). Paralympic sport: an emerging area for research and consultancy in sports biomechanics. Sports Biomech, 10, 249–268.

Rudins, A., Laskowski, E. R., Growney, E. S., Cahalan, T. D., & An, K. N. (1997). Kinematics of the elbow during wheelchair propulsion: a comparison of two wheelchairs and two stroking techniques. Archives of physical medicine and rehabilitation, 78(11), 1204-1210.

Gehlsen, G. M., Davis, R. W., & Bahamonde, R. (1990). Intermittent velocity and wheelchair performance characteristics. Adapted Physical Activity Quarterly, 7(3), 219-230.

Coutts, K. D. (1990). Kinematics of sport wheelchair propulsion. Journal of rehabilitation research and development, 27(1), 21-26.

Fuss, F. K. (2009). Influence of mass on the speed of wheelchair racing. Sports Engineering, 12(1), 41-53.

LaMere, T.J., & Labanowich, S. (1984). The history of sports wheelchairs: Part III, The racing wheelchair 1976-1983. Sports 'n Spokes, 10 (1), 12-16.

Barbosa, T. M., Forte, P., Morais, J. E., Coelho, E. (2014). Partial contribution of rolling friction and drag force to total resistance of an elite wheelchair athlete. 1st International Conference in Sports Sciences & Technology. ICSST, Advanced Materials for Sport Technology, 749-753.

Burke, E. (Ed.). (1986). Science of cycling. Champaign, IL: Human Kinetics Publishers.

Hedrick, B., Wang, Y. T., Moeinzadeh, M., & Adrian, M. (1990). Aerodynamic positioning and performance in wheelchair racing. Adapted Physical Activity Quarterly, 7(1).

FIFA. (2001). Quality Concept for Football Turf. Available: http://www.fifa.com/mm/document/afdeveloping/pitchequip/fqc_football_turf_folder_342.pdf.

Kolitzus, H. J. (2003). Ball Roll Behavior: The Functional Relationship of the Ball Roll Distance and the Timing Gate Method; How to Calculate the Ball Roll Distance from Timing Gate Measurements. ISSS - International Association for Sports Surface Sciences, Eschenz / Switzerland, Available: http://www.isss-sportsurfacescience.org/downloads/documents/ZPKPAJJUWY_Ball_Roll_BehaviorKS.pdf.

Kwarciak, A. M., Yarossi, M., Ramanujam, A., Dyson-Hudson, T. A., & Sisto, S. A. (2009). Evaluation of wheelchair tire rolling resistance using dynamometer-based coast-down tests. J Rehabil Res Dev, 46(7), 931-38.

DiGiovine, C. P., Cooper, R. A., Boninger, M. L. (2001). Dynamic calibration of a wheelchair dynamometer. J Rehabil Res Dev, 38(1), 41–55.

Candau, R. B., Grappe, F., Menard, M., Barbier, B., Millet, G.Hoffman, M. D. (1999). Simplified deceleration method for assessment of resistive forces in cycling. Medicine and Science in Sports and Exercise, 31, 1441–1447.

MacLeish, M. S., Cooper, R. A., Harralson, J., & Ster, J. F. (1993). Design of a composite monocoque frame racing wheelchair. Journal of rehabilitation research and development, 30, 233-233.

Burton, M., Fuss, F. K., & Subic, A. (2010). Sports wheelchair technologies. Sports Technology, 3(3), 154-167.

Petrushov, V. A. (1998). Improvement in vehicle aerodynamic drag and rolling resistance determination from coast-down tests. Proceedings of the Institution of Mechanical Engineers, Part D: Journal of Automobile Engineering, 212(5), 369-380.

Hanna, R. K. (2012). CFD in Sport-a Retrospective; 1992-2012. Procedia Engineering, 34, 622-627.

Marinho, D. A., Barbosa, T. M., Mantha, V., Rouboa, A. I., & Silva, A. J. (2012). Modelling propelling force in swimming using numerical simulations. In: Juarez LH (Ed). Fluid Dynamics, Computational Modeling and Applications. 439-448. InTech. Rijeka.

Marinho, D.A., Silva, A.J., Reis, V.M., Barbosa, T. M., Vilas-Boas, J.P., Alves, F.B., Machado, L., Rouboa, A. (2011) Three-dimensional CFD analysis of the hand and forearm in swimming. Journal of Applied Biomechanics. ISSN 1065-8483. 27(1), 74-80.

Caboz, E. B. (2010). Simulação computacional do escoamento em torno de um capacete de ciclista usado nas provas de contra-relógio. Dissertação de mestrado. Faculdade de Engenharia da Universidade do Porto.

White, F. (1999). Mecanica dos Fluidos, Ed. McGraw -Hill, 4ª edição. ISBN : 85-86804-24-X.

Carvalho, F. (2008). A aplicação da dinâmica computacional de fluidos no estudo do arrasto hidrodinâmico na natação. Dissertação de Mestrado em Educação Fisica e Desporto. Universidade de Trás os Montes. Vila Real.

Pinnoji, P. K., & Mahajan, P. (2006). Impact analysis of helmets for improved ventilation with deformable head model. In Proceeding of IRCOBI conference, Madrid, 159-70.

Rushby-Smith, T., & Douglas, L. (2012). Paralympic Technology. Ingenia, 51, 33.

Chapter 3. Comparison by computer fluid dynamics of the drag force acting upon two helmets for wheelchair racers.

Martin, P. (2009). Computational Fluid Dynamics for Sport Simulation, Springer.

LaMere, T. J. & Labanowich, S. (1984). “The history of sports wheelchairs: Part III, The racing wheelchair 19761983”. Sports ‘n Spokes, 10(1), 12-16.

Alam, F., Chowdhury, H., Wei, H. Z., Mustary, I. & Zimmer, G. (2014). “Aerodynamics of ribbed bicycle racing helmets”. Procedia engineering, 72, 691-696.

Rushby-Smith, T. & Douglas, L. (2012). Paralympic Technology. Ingenia, 51, 33.

Forte, P., Barbosa, T. M., & Marinho, D. A. (2015). “Technologic Appliance and Performance Concerns in Wheelchair Racing – Helping Paralympic Athletes to Excel” in New Perspectives in Fluid Dynamics, edited by Dr. Chaoqun Liu, 101-121. InTech.

Marinho, D. A., Barbosa, T. M., Mantha, V., Rouboa, A. I., & Silva, A. J. (2012) “Modelling propelling force in swimming using numerical simulations” in Fluid Dynamics, Computational Modeling and Applications, edited by Juarez LH, 439-448. InTech.

Marinho, D. A., Silva, A. J., Reis, V. M., Barbosa, T. M., Vilas-Boas, J. P., Alves, F. B., Machado, L., Rouboa. A. (2011) “Three-dimensional CFD analysis of the hand and forearm in swimming”. Journal of Applied Biomechanics, 27(1), 74-80.

Sanders, R. H. (1999). “Hydrodynamic characteristics of a swimmer’s hand”. Journal of Applied Biomechanics, 15(1), 3–26.

Aroussi, A., Kucukgokoglan, S., Pickering, S. J., Menacer, M. (2001). “Evaluation of four turbulence models in the interaction of multi burners swirling flows” in 4th International Conference On Multiphase Flow. New Orleans, Louisiana, USA.

Sidelko, S. (2007). “Benchmark of aerodynamic cycling helmets using a refined wind tunnel test protocol for helmet drag research” Doctoral dissertation, Massachusetts Institute of Technology.

Chapter 4. The variations on the aerodynamics of a world-ranked wheelchair sprinter in the key-moments of the stroke cycle: a numerical simulation analysis.

Forte, P., Marinho, D. A., Morouço, P., Pascoal-Faria, P. & Barbosa T. M. 2017. Comparison by computer fluid dynamics of the drag force acting upon two helmets for wheelchair racers. AIP Conference Proceedings, AIP Publishing. 1863 (1): 520005-520008.

Forte, P., Barbosa, T. M. & Marinho, D. A. 2015. Technologic Appliance and Performance Concerns in Wheelchair Racing – Helping Paralympic Athletes to Excel. New Perspectives in Fluid Dynamics, Chaoqun Liu (Ed.), InTech, 101-121.

Fuss, F. K. 2009. Influence of mass on the speed of wheelchair racing. Sports Engineering, 12 (1): 41-53.

Cooper, R. A. 1990. Wheelchair racing sports science: a review. Journal of Rehabilitation research and development. 27(3): 295-312.

Candau, R., Grappe, F., Menard, M., Barbier, B., Millet, G. P., Hoffman, M. D, et al. 1999. Simplified deceleration method for assessment of resistive forces in cycling. Medicine and Science in Sports and Exercise, 31: 1441–1447.

di Prampero, P. E. 1986. The energy cost of human locomotion on land and in water. International Journal of Sports and Medicine, 7: 55–72.

Martin, J. C., Gardner, A. S., Barras, M. & Martin, D. T. 2006. Modelling sprint cycling using field-derived parameters and forward integration. Medicine and Science in Sports and Exercise, 38: 592 –597.

Millet, G. P. & Candau, R. 2002. Mechanical factors of the energy cost in three human locomotions. Science & Sports, 17: 166–176

Barbosa, T. M., Forte, P., Morais, J. E. & Coelho, E. 2014. Partial contribution of rolling friction and drag force to total resistance of an elite wheelchair athlete. Proc. 1st Int. Conf. in Sports Sciences & Technology (Singapore: Institute of Sports Research), 749-53.

Ryschon T, W. & Stray-Gundersen, James. 1991. The effect of body position on the energy cost of cycling. Medicine and Science in Sports and Exercise, 23(8): 949-953.

McLean, B. D., Danaher, R., Thompson, L., Forges, A. & Coco, G. 1994. Aerodynamic characteristics of cycle wheels and racing cyclists. Journal of Biomechanics, 27: 675.

Paton, C. 2006. Aerodynamic drag area of cyclists determined with field-based measures. Sportscience, 10: 69-71.

Barbosa, T. M., Forte, P., Estrela, J. E. & Coelho, E. 2016. Analysis of the aerodynamics by experimental testing of an elite wheelchair sprinter. Procedia Engineering, 147: 2-6.

Schlichting, H. Boundary Layer Theory. McGraw-Hill. New York. 1979.

Debraux, P., Grappe, F., Manolova, A. V. & Bertucci, W. 2011. Aerodynamic drag in cycling: methods of assessment. Sports Biomechanics, 10(3): 197-218.

Kennedy, M. D. & Lamo, W. D. 2013. Applied ergonomics of cycling performance. Routledge handbook of ergonomics in sport and exercise. Hong Y. (Ed.), Routledge. London, 115-127.

Kyle, C. R. 2013. Selecting cycling equipment. High-Tech Cycling, Burke ER (Ed), Human Kinetics, 1–48, Champaign, IL.

Harun, C. 2012. Aerodynamic Design of Sports Garments. Applied Aerodynamics. Jorge Colman Lerner (Ed.), InTech. Rijeka, 21-40.

Defraeye, T., Blocken, B., Koninckx, E., Hespel, P. & Carmeliet, J. 2012. Computational fluid dynamics analysis of cyclist aerodynamics: Performance of different turbulence-modelling and boundary-layer modelling approaches. Journal of biomechanics, 43(12): 2281-2287.

Kulfan, B. 2007. Assessment of CFD predictions of viscous drag. Fluids 2000 Conference and Exhibit, Fluid Dynamics. American Institute of Aeronautics and Astronautics-2000-2391, 2-36.

Edwards, A. G. & Byrnes, W. C. 2007. Aerodynamic characteristics as determinants of the drafting effect in cycling. Medicine and science in sports and exercise, 39(1): 170-176.

Crouch, T. N., Burton, D., LaBry, Z. A. & Blair, K. B. 2017. Riding against the wind: a review of competition cycling aerodynamics. Sports Engineering, 20(2): 81-110.

Bouillod, A., Oggiano, L., Soto-Romero, G., Brunet, E. & Grappe, F. 2016. Preliminary study: A new method to assess the effective frontal area of cyclists. 4th International Congress on Sport Sciences Research and Technology Support (IcSPORTS), Jan Cabri, João Paulo Vilas-Boas, Pedro Pezarat Correia (Eds.), 1-6.

Hoffman, M. D., Millet, G. Y., Hoch, A. Z. & Candau, R. B. 2003. Assessment of wheelchair drag resistance using a coasting deceleration technique. American Journal of Physical Medicine & Rehabilitation, 82(11): 880-889.

Pogni, M. & Nicola, P. Comparison of the Aerodynamic Performance of Five Racing Bicycle Wheels by Means of CFD Calculations. Procedia Engineering, 147: 74-80.

Bixler, B., Pease, D. & Fairhurst, F. 2007. The accuracy of computational fluid dynamics analysis of the passive drag of a male swimmer, 6(1): 81–98.

Marinho, D. A., Barbosa, T. M., Reis, V. M., Kjendlie, P. L., Alves, F. B., Vilas-Boas, J. P., et al. 2010. Swimming propulsion forces are enhanced by a small finger spread. Journal of Applied Biomechanics, 26(1): 87–92. 2010.

ANSYS Inc-. 2013. Introduction to Using ANSYS FLUENT in ANSYS Workbench: Fluid Flow and Heat Transfer in a Mixing Elbow. ANSYS Fluent Tutorial Guide, Release 15.0. ANSYS Inc (eds). EUA, 1-74.

Winkler, A. & Pernpeintner, A. 2010. Automated aerodynamic optimization of the position and posture of a bobsleigh crew. Procedia Engineering, 2(2): 2399-405.

Defraeye, T., Blocken, B., Koninckx, E., Hespel, P. & Carmeliet, J. 2010. Aerodynamic study of different cyclist positions: CFD analysis and full-scale wind-tunnel tests. Journal of Biomechanics, 43 7: 1262-1268.

Blocken, B., Defraeye, T., Koninckx, E., Carmeliet, J. & Hespel, P. 2013. CFD simulations of the aerodynamic drag of two drafting cyclists. Computers & Fluids, 71: 435-445.

Griffith, M. D., Crouch, T., Thompson, M. C., Burton, D., Sheridan, J. & Brown, N. A. 2014. Computational fluid dynamics study of the effect of leg position on cyclist aerodynamic drag. Journal of Fluids Engineering, 136(10): 101105.

Grappe, F., Candau, R., Belli, A. & Rouillon, J. D. 1997. Aerodynamic drag in field cycling with special reference to the Obree's position. Ergonomics, 40 (12): 1299-1311.

Defraeye T., Blocken, B., Koninckx, E., Hespel, P., Verboven, P., Nicolai, B. & Carmeliet, J. 2014. Cyclist drag in team pursuit: influence of cyclist sequence, stature and arm spacing. Journal of Biomechanical Engineering, 136(1): 011005.

Faria, E. W., Parker, D. L. & Faria, I. E. 2005. The science of cycling: Factors affecting performance – Part 2. Sports Medicine, 35: 313 –337.

Barbosa, T. M., Morais, J. E., Forte, P., Neiva, H., Garrido, N. D. & Marinho, D. A. 2017. A Comparison of Experimental and Analytical Procedures to Measure Passive Drag in Human Swimming. PloS One, 12(5): e0177038.

Munson, B. R., Young, D. F. & Okiishi, T. H. 1990. Fundamentals of Fluid Mechanics. Wiley. New York.

Ridgway, M., Pope, C. & Wilkerson, J. 1988. A kinematic analysis of 800-meter wheelchair racing techniques. Adapted Physical Activity Quarterly, 5(2): 96-107.

Gehlsen, G. M., Davis, R. W. & Bahamonde, R. Intermittent velocity and wheelchair performance characteristics. Adapted Physical Activity Quarterly, 7(3): 219-230.

Cooper, R. A. 1990. An exploratory study of racing wheelchair propulsion dynamics. Adapted Physical Activity Quarterly, 7(1): 74-85.

Sanderson, D. J. & Sommer, H. J. 1985. Kinematic features of wheelchair propulsion. Journal of Biomechanics. 18(6): 423-429.

Aroussi, A., Kucukgokoglan, S., Pickering, S. J., Menacer, M. (2001). “Evaluation of four turbulence models in the interaction of multi burners swirling flows” in 4th International Conference On Multiphase Flow. New Orleans, Louisiana, USA.

Chapter 5. Estimation of mechanical power and energy cost in elite wheelchair racing by analytical procedures and numerical simulations.

Abel, T., Kröner, M., Rojas, V. S., Peters, C., Klose, C., Platen, P. (2003). Energy expenditure in wheelchair racing and handbiking-a basis for prevention of cardiovascular diseases in those with disabilities. European Journal of Cardiovascular Prevention & Rehabilitation. 10(5): 371-376.

ANSYS Fluent. (2013). ANSYS Fluent, Release 15.0, Theory Guide, ANSYS Inc.

Barbosa, T. M., Coelho, E. (2017). Monitoring the biomechanics of a wheelchair sprinter racing the 100 m final at the 2016 Paralympic Games. European Journal of Physics. 38.4: 044001.

Barbosa, T. M., Forte, P., Estrela, J. E., Coelho, E. (2016). Analysis of the aerodynamics by experimental testing of an elite wheelchair sprinter. Procedia Engineering. 147: 2-6.

Barbosa, T. M, Forte, P., Morais, J. E, Coelho, E. (2014). Partial contribution of rolling friction and drag force to total resistance of an elite wheelchair athlete. Proceedings of the 1st International Conference in Sports Science & Technology. Singapore: Institute of Sports Research. 749-53.

Bixler, B., Pease, D., Fairhurst, F. (2007). "The accuracy of computational fluid dynamics analysis of the passive drag of a male swimmer". Sports Biomechanics. 6(1): 81–98.

Blocken, B., Toparlar, Y., & Andrianne, T. (2016). Aerodynamic benefit for a cyclist by a following motorcycle. Journal of Wind Engineering and Industrial Aerodynamics. 155: 1-10.

Candau, R. B., Grappe, F. R., Ménard, M. A., Barbier, B. R., Millet, G. Y., Hoffman, M. D., Belli, A. R., Rouillon, J. D. (1999). Simplified deceleration method for assessment of resistive forces in cycling. Med Sci Sports Exerc. 31: 1441-7.

Chua, J. J., Fuss, F. K., Subic, A. (2010). Rolling friction of a rugby wheelchair. Procedia Eng. 2(2): 3071-6

Cooper, R. A., Boninger, M. L., Cooper, R., Robertson, R. N., Baldini, F. D. (2003). Wheelchair racing efficiency. Disability and rehabilitation. 1(25): 207-12

Forte, P., Barbosa, T. M., Marinho, D. A. (2015). “Technologic Appliance and Performance Concerns in Wheelchair Racing – Helping Paralympic Athletes to Excel”. New Perspectives in Fluid Dynamics, Dr. Chaoqun Liu (Ed.). InTech. 101-121.

Forte, P., Marinho, D. A., Morouço, P. G., Barbosa, T. (2016). CFD analysis of head and helmet aerodynamic drag to wheelchair racing. In Technology and Innovation in Sports, Health and Wellbeing (TISHW), International Conference. IEEE. 1-6.

Fuss, F. K. (2009). Influence of mass on the speed of wheelchair racing. Sports Engineering. 12: 41-53.

Hoffman, M. D., Millet, G. Y., Hoch, A. Z., Candau, R. B. (2003). Assessment of wheelchair drag resistance using a coasting deceleration technique. Am J Physical Med & Rehab. 82(11): 880-9

MacLeish, M. S., Cooper, R. A., Harralson, J., Ster, J. F. (1993). Design of a composite monocoque frame racing wheelchair. Journal of rehabilitation research and development. 30: 233-233.

Marinho, D. A., Barbosa, T. M., Mantha, V., Rouboa, A. I., Silva, A. J. (2012). “Modelling propelling force in swimming using numerical simulations”. In: Juarez LH (Ed). Fluid Dynamics, Computational Modeling and Applications. InTech. 439-448.

Marinho, D. A., Barbosa, T. M., Reis, V. M., Kjendlie, P. L., Alves, F. B., Vilas-Boas, J. P., et al. (2010). “Swimming propulsion forces are enhanced by a small finger spread”. Journal of Applied Biomechanics. 26(1): 87–92.

Marinho, D. A., Silva, A. J., Reis, V. M., Barbosa, T. M., Vilas-Boas, J. P., Alves, F. B., Machado, L., Rouboa, A. (2011). “Three-dimensional CFD analysis of the hand and forearm in swimming”. Journal of Applied Biomechanics. 27(1): 74-80.

Martin, J. C. (1996). Aerodynamics and cycling. Master Athlete Physiology and Performance.

McLean, B. D., Danaher, R., Thompson, L., Forges, A., Coco, G. (1994). Aerodynamic characteristics of cycle wheels and racing cyclists. In Journal of Biomechanics. 27: 675.

Pelland-Leblanc, J. P., Martel, F., Langelier, È., Smeesters, C., Berrigan, F., Laroche, J., Rancourt, D. (2013). Instantaneous power measurement in wheelchair racing. In 37th Annual Meeting of the American Society of Biomechanics. Omaha, Nebraska, USA.

Pogni, M., Nicola, P. (2016). "Comparison of the Aerodynamic Performance of Five Racing Bicycle Wheels by Means of CFD Calculations." Procedia Engineering. 147: 74-80.

Rushby-Smith, T., Douglas, L. (2012). Paralympic Technology. Ingenia. 51: 33.

Ryschon, T. W., Stray-Gundersen, J. A. M. E. S. (1991). The effect of body position on the energy cost of cycling. Medicine and science in sports and exercise. 23(8): 949-953.

Sauret, C., Bascou, J., de Saint Rémy, N., Pillet, H., Vaslin, P., Lavaste, F. (2012). Assessment of field rolling resistance of manual wheelchairs. J Rehab Res Development. 49(1): 63-74.

Theisen, D., Francaux, M., Fay, A., Sturbois, X. (1996). A new procedure to determine external power output during handrim wheelchair propulsion on a roller ergometer: a reliability study. International journal of sports medicine. 17(08): 564-571.

Vanlandewijck, Y. C., & Thompson, W. R. (2011). Handbook of sports medicine and science, the paralympic athlete. John Wiley & Sons.

Wilson, D. G. (2004). Bicycle aerodynamics. In: Bicycling science. Cambridge, MA: MIT Press. 188.

Chapter 6. General Discussion

Fuss, F. K. (2009). Influence of mass on the speed of wheelchair racing. Sports Engineering. 12: 41-53.

Forte, P., Barbosa, T. M., Marinho, D. A. (2015). “Technologic Appliance and Performance Concerns in Wheelchair Racing – Helping Paralympic Athletes to Excel”. New Perspectives in Fluid Dynamics, Dr. Chaoqun Liu (Ed.). InTech. 101-121.

MacLeish, M. S., Cooper, R. A., Harralson, J., Ster, J. F. (1993). Design of a composite monocoque frame racing wheelchair. Journal of rehabilitation research and development. 30: 233-233.

Barbosa, T. M., Coelho, E. (2017). Monitoring the biomechanics of a wheelchair sprinter racing the 100 m final at the 2016 Paralympic Games. European Journal of Physics. 38.4: 044001.

Barbosa, T. M., Forte, P., Estrela, J. E., Coelho, E. (2016). Analysis of the aerodynamics by experimental testing of an elite wheelchair sprinter. Procedia Engineering. 147: 2-6.

Barbosa, T. M, Forte, P., Morais, J. E, Coelho, E. (2014). Partial contribution of rolling friction and drag force to total resistance of an elite wheelchair athlete. Proceedings of the 1st International Conference in Sports Science & Technology. Singapore: Institute of Sports Research. 749-53.

Pinnoji, P. K., & Mahajan, P. (2006). Impact analysis of helmets for improved ventilation with deformable head model. In Proceeding of IRCOBI conference, Madrid, 159-70.

Rushby-Smith, T., Douglas, L. (2012). Paralympic Technology. Ingenia. 51: 33.

Winkler, A., Pernpeintner, A. (2010). Automated aerodynamic optimization of the position and posture of a bobsleigh crew. Procedia Engineering. 2(2):2399-405.

Blocken, B., Defraeye, T., Koninckx, E., Carmeliet, J., & Hespel, P. (2013). CFD simulations of the aerodynamic drag of two drafting cyclists. Computers & Fluids, 71, 435-445.

Griffith, M. D., Crouch, T., Thompson, M. C., Burton, D., Sheridan, J., & Brown, N. A. (2014). Computational fluid dynamics study of the effect of leg position on cyclist aerodynamic drag. Journal of Fluids Engineering, 136 (10), 101105.

Grappe, F., Candau, R., Belli, A., & Rouillon, J. D. (1997). Aerodynamic drag in field cycling with special reference to the Obree's position. Ergonomics, 40 (12), 1299-1311.

Defraeye, T., Blocken, B., Koninckx, E., Hespel, P., & Carmeliet, J. (2010). "Aerodynamic study of different cyclist positions: CFD analysis and full-scale wind-tunnel tests." Journal of biomechanics 43.7: 1262-1268.

Defraeye, T., Blocken, B., Koninckx, E., Hespel, P., Verboven, P., Nicolai, B., Carmeliet, J. (2014). Cyclist drag in team pursuit: influence of cyclist sequence, stature and arm spacing, Journal of Biomechanical Engineering 136 (1), 011005.

Millet, G. P., & Candau, R. (2002). Facteurs mécaniques du cout énergétique dans trios locomotions humaines [Mechanical factors of the energy cost in three human locomotions]. Science & Sports, 17, 166–176. Retrieved from http://www.em-consulte.com/article/24078.

Faria, E. W., Parker, D. L., & Faria, I. E. (2005). The science of cycling: Factors affecting performance – Part 2. Sports Medicine, 35, 313 –337. Retrieved from http://adisonline.com/sportsmedicine/Abstract/2005/35040/The_Science_of_Cycling__Factors_Affecting.3.aspx

Hoffman, M. D., Millet, G. Y., Hoch, A. Z., Candau, R. B. (2003). Assessment of wheelchair drag resistance using a coasting deceleration technique. Am J Physical Med & Rehab. 82(11): 880-9

Rushby-Smith, T. & Douglas, L. (2012). Paralympic Technology. Ingenia, 51, 33.

McLean, B. D., Danaher, R., Thompson, L., Forges, A., Coco, G. (1994). Aerodynamic characteristics of cycle wheels and racing cyclists. In Journal of Biomechanics, 27, 675.

Martin, J. C. (1996). Aerodynamics and cycling. Master Athlete Physiology and Performance.

Blocken, B., Toparlar, Y., & Andrianne, T. (2016). Aerodynamic benefit for a cyclist by a following motorcycle. Journal of Wind Engineering and Industrial Aerodynamics. 155: 1-10.

ANSYS Fluent. (2013). ANSYS Fluent, Release 15.0, Theory Guide, ANSYS Inc.

Cooper, R. A., Boninger, M. L., Cooper, R., Robertson, R. N., Baldini, F. D. (2003). Wheelchair racing efficiency. Disability and rehabilitation. 1(25): 207-12

Candau, R. B., Grappe, F. R., Ménard, M. A., Barbier, B. R., Millet, G. Y., Hoffman, M. D., Belli, A. R., Rouillon, J. D. (1999). Simplified deceleration method for assessment of resistive forces in cycling. Med Sci Sports Exerc. 31: 1441-7.

Pelland-Leblanc, J. P., Martel, F., Langelier, È., Smeesters, C., Berrigan, F., Laroche, J., Rancourt, D. (2013). Instantaneous power measurement in wheelchair racing. In 37th Annual Meeting of the American Society of Biomechanics. Omaha, Nebraska, USA.

Abel, T., Kröner, M., Rojas, V. S., Peters, C., Klose, C., Platen, P. (2003). Energy expenditure in wheelchair racing and handbiking-a basis for prevention of cardiovascular diseases in those with disabilities. European Journal of Cardiovascular Prevention & Rehabilitation. 10(5): 371-376.

Theisen, D., Francaux, M., Fay, A., Sturbois, X. (1996). A new procedure to determine external power output during handrim wheelchair propulsion on a roller ergometer: a reliability study. International journal of sports medicine. 17(08): 564-571.